Boundary-Layer Meteorology (2024) 190:44
https://doi.org/10.1007/s10546-024-00877-7

RESEARCH ARTICLE

Spectral Properties of Turbulence in a Suburban Area of São Paulo Megacity

Lucas Cardoso da Silveira[1] · Amauri Pereira de Oliveira[1] · Georgia Codato[1] · Maciel Piñero Sánchez[1] · Adalgiza Fornaro[1]

Received: 5 September 2023 / Accepted: 14 July 2024 / Published online: 24 September 2024
© The Author(s), under exclusive licence to Springer Nature B.V. 2024

Abstract
Turbulence has a significant impact on the urban climate, affecting the well-being of millions of people living in cities. Spectral analysis is useful for understanding turbulent processes. However, there are gaps in the knowledge of turbulence spectral properties over urban surfaces, especially processes involving passive gases. In this study, turbulence spectral properties are investigated within the Monin–Obukhov similarity theory framework. In situ turbulence measurements of wind velocity components, temperature, and water vapor and carbon dioxide densities were carried out at 25–26 m above ground between 2009 and 2017 in a suburban area of the Metropolitan Region of São Paulo, Brazil. Our results indicated that the spectra (cospectra) of velocity and scalars followed the − 2/3 (− 4/3) slope in the inertial subrange. Under neutral conditions, the cospectra of the passive gases were nearly identical. The normalized dissipation rates of turbulent kinetic energy and scalar variances, as well as fluxes, can be described by similarity functions based on the local equilibrium assumption when the imbalance factors were considered. In addition, the similarity functions for the normalized dissipation rates of the water vapor and CO_2 variances were nearly identical. A more suitable similarity function for the normalized dissipation rate of temperature variance in urban areas was proposed. The spectra of the passive gases exhibited a minor peak in the low-frequency range possibly associated with non-local effects. These results enhance our understanding of the turbulent exchanges in urban environments and can contribute to air quality assessment and engineering applications.

Keywords Dissipation rate of the scalar variance · Dissipation rate of the turbulent kinetic energy · Monin–Obukhov similarity theory · Turbulence spectra · Urban climate

1 Introduction

Turbulent exchange processes involving mass, heat, and momentum on urban surfaces play important roles in the microclimate of cities. Their understanding provides engineering strategies with respect to thermal and wind comfort (e.g., Toparlar et al. 2015; Taleghani et al.

✉ Lucas Cardoso da Silveira
lucas.silveira@alumni.usp.br

[1] Department of Atmospheric Science, University of São Paulo, São Paulo 05508-090, Brazil

2016; Stuck et al. 2021), improvements in pollutant dispersion modeling (e.g., Garbero et al. 2010; Falabino and Trini Castelli 2017; Liu et al. 2023), and other important issues of the urban climate that directly influence human health and well-being. Spectral analysis is a powerful tool for investigating turbulent transfers between urban surfaces and the overlying atmosphere (Clarke et al. 1982; Högström et al. 1982; Roth and Oke 1993; Rotach 1995; Oikawa and Meng 1995; Feigenwinter et al. 1999; Zhang et al. 2001; Roth et al. 2006; Fortuniak and Pawlak 2015; Ramamurthy and Pardyjak 2015). However, turbulence spectral properties in urban areas are poorly documented and require further observational studies (Roth 2000).

Over homogeneous surfaces, the spectrum of turbulent kinetic energy (TKE) obeys the Kolmogorov empirical laws (Frisch 1995). Estimated from the Fourier Transform of autocovariance of wind speed, the wavenumber of the TKE spectrum can be substituted by frequency ever since the frozen-turbulence Taylor's hypothesis is satisfied by the turbulent flow. This variable change allows to estimate the TKE spectrum in the atmosphere from time series of the wind speed components measured in a fixed-point with high sampling rates ($\geq$ 1 Hz). In general, the TKE spectrum can be characterized by a maximum (spectral peak) within the energy-containing range at low frequencies, an inertial subrange where the spectrum intensity decays proportional to frequency raised to $-$ 5/3 power, and a dissipation range. Similar spectral properties are observed for each individual velocity components and scalars such as temperature, water vapor and carbon dioxide densities. By analogy, the Kolmogorov empirical laws apply to the cospectrum. It corresponds to the Fourier transfor of cross-covariance between wind speed components (representing vertical turbulent fluxes of horizontal wind components) and scalars (representing vertical turbulent fluxes of temperature, water vapor and carbon dioxide). The cospectrum displays a spectral peak in the energy containing at low-frequency range, decays proportional to frequency raised to $-$ 5/3 power in the inertial subrange. It becomes zero in the dissipation range due to the strong impact of local isotropy (Stull 1988; Wyngaard 2010).

Even though the Kolmogorov empirical laws still hold over heterogenous surface, such as urban areas, some differences have been reported in the literature. In terms of shape and peak location, the velocity spectra and cospectra on urban surfaces are similar to the reference data obtained by Kaimal et al. (1972) for homogeneous surfaces (Högström et al. 1982; Roth and Oke 1993; Rotach 1995; Feigenwinter et al. 1999; Roth et al. 2006; Fortuniak and Pawlak 2015). In addition, Fortuniak and Pawlak (2015) reported that the normalized dissipation rate of TKE derived from velocity spectra could also be described by similarity functions based on the local equilibrium assumption in urban areas. In contrast with homogeneous surfaces, however, they verified that there was no 'excluded region' for horizontal velocity spectra, indicating a continuous transition from stable to unstable conditions (cf. Kaimal et al. 1972). Another urban spectrum particularity is the peak shift of the vertical velocity toward lower frequencies corresponding to length scales on the order of the mean building height; this result indicates that most of the vertical transport in urban areas is due to the eddies produced by building wakes and coherent structure-induced sweeps and ejections produced by inflection point instability of the vertical wind speed profile on building roofs (Roth 2000; Christen et al. 2009).

On the other hand, information regarding the spectral properties of scalars in urban areas is scarce in the literature. Consequently, the behavior of scalar spectra, especially the density of passive gases such as water vapor and carbon dioxide, remains unclear. Temperature spectra show similarities with homogeneous surface data under unstable conditions (Roth and Oke 1993; Roth 2000; Roth et al. 2006). However, Clarke et al. (1982) noted a significant mesoscale component for neutral and stable spectra of temperature. Similarly, Roth and

Oke(1993) results indicated that humidity transfer was influenced by large-scale structures in urban areas, which affected the spectra in the low-frequency range. Indeed, the influence of mesoscale motions on the turbulence structure over urban surfaces could lead to an enhanced turbulence, contributing to the turbulent transport of mass from upper layers to the surface and vice versa (e.g., Westcott 1989).

Ramamurthy and Pardyjak (2015) reported that large-scale advection processes influenced the CO_2 turbulent transport at lower frequencies under stable conditions. Roth et al. (2003) reasoned that local sources and sinks strongly influenced the CO_2 spectra and cospectra under unstable conditions, contributing to little or no spectral drop-off at lower frequencies. Finally, under particular atmospheric conditions (e.g., low-wind speed), the peak observed for the turbulence spectra of temperature, as well as for horizontal velocity components, at lower frequencies could be associated with submeso motions on urban surfaces, such as meandering (Mortarini and Anfossi 2015; Mortarini et al. 2016). In addition, some evidence implied that scalar spectra were independent of atmospheric stability in urban areas (e.g., Roth et al. 1999; Zhang et al. 2001). This suggests that the scalar spectra could be driven by other scales in the low-frequency range.

In regard to the normalized dissipation rates of the scalar variance and flux, the applicability of the usual similarity functions for homogeneous surfaces (e.g., Kaimal et al. 1972; Ohtaki 1985) is debatable, and 'urban forms' are needed to better describe the data from urban environments (Roth and Oke 1993; Roth et al. 2006). In addition, the influence of the individual roughness elements (such as buildings and trees) on turbulence measurements, or nonlocal emission sources and sinks that characterize the roughness sublayer (RSL), which is the lower part of the surface layer, limits the applicability of the Monin–Obukhov similarity theory (MOST) and raises questions regarding the validity of universal functions in an urban context (Fortuniak and Pawlak 2015; Silveira et al. 2022).

Based on the above considerations, understanding spectral properties in urban environments is important. Unfortunately, the few turbulent flux observations of momentum, heat, and water vapor or CO_2 density over urban surfaces are not sufficient to completely understand the turbulent exchange processes of these atmospheric properties.

In this study, an observational investigation of the spectral properties of turbulence over a suburban surface in the Metropolitan Region of São Paulo, Brazil, was conducted between 2009 and 2017 using in situ turbulence measurements of wind velocity components, temperature, and water vapor and CO_2 densities. The spectra and cospectra of velocity and scalars were analyzed within the Monin–Obukhov similarity theory framework. The universal constants and normalized dissipation rates were evaluated, and spectral analytical models were tested. The site and instrumentation are described in Sect. 2. The results are presented and discussed in Sect. 3. The main findings and conclusions are highlighted in Sect. 4.

2 Methodology

2.1 Site, Climate, and Instrumentation

The Metropolitan Region of São Paulo (MRSP) is located in the southeastern region of Brazil. It is situated on a plateau at 722 m above mean sea level (a.m.s.l.) and 65 km inland from the Atlantic Ocean. According to IBGE (2018), the MRSP is the most populated Brazilian-metropolitan area and encompasses approximately 22 million inhabitants.

Generally, the climate of the MRSP is characterized by dry and mildly cold winters (June–August) and wet and warm summers (December–March). It is classified as high-elevation subtropical humid (Cwb) based on the Köppen classification (Oliveira et al. 2003; Sánchez et al. 2020). Thermal (sea breeze, mountain-valley, and urban heat island) and mechanical (channeling, roughness, and building-barrier) circulations modulate the spatial and temporal variation of the surface wind flow (Ribeiro et al. 2018; Umezaki et al. 2020; Oliveira et al. 2020). Synoptic and mesoscale systems on the MRSP impact the temporal evolution of the urban boundary layer (UBL). Cloudiness patterns associated with synoptic and mesoscale disturbances yield shallow and shear-driven UBLs during the day, whereas radiative cooling reduction due to clouds favors deeper stable boundary layer (SBL) development at night (Sánchez et al. 2020). In addition, the sea breeze passage at the MRSP disrupts UBL evolution by establishing a thermal internal boundary layer (Ribeiro et al. 2018). Further information on the MRSP climate and its dominant features can be found in Oliveira et al. (2020) and Sánchez et al. (2022).

According to Sanchéz et al. (2020), during the daytime, the UBL height in the MRSP displays seasonal variation, with a minimum of 1061 m in September (spring) and a maximum of 1,632 m in May (fall), based on rawinsonde analysis. During the night-time, the maximum SBL height ranges from 122 m in winter to 126 m in summer. In the winter, the spatial variation in the UBL height at the MRSP is mainly controlled by the cloud effects and afternoon sea breeze intrusions (Sanchéz et al. 2020). Additionally, lidar observations during winter months have indicated that under less disturbed synoptic conditions, the UBL height displays mesoscale horizontal variations within the urban limits (~ 20 km) of up to 300 m due to the topographic effects (Moreira et al. 2022). The surface layer, comprized of by the RSL and the overlying inertial sublayer (ISL), corresponds to 12% of the UBL in winter and 10% in summer at the MRSP (Sánchez et al. 2020).

Turbulence measurements were conducted on the micrometeorological platform at the Institute of Astronomy, Geophysics and Atmospheric Science (PM IAG) from the University of São Paulo (23° 33 ′34 ″ S, 46° 44 ′01 ″ W, 744 m a.m.s.l.). It is situated in the western part of São Paulo City and integrates the micrometeorological observation network from the MCITY BRAZIL project (Oliveira et al. 2020). The platform is on the rooftop of a three- to four-story building and encompasses a turbulence data acquisition system set up on a 10 m tower (Fig. 1a). The turbulence data consist of the three wind components (u, v, w), sonic temperature (T), and densities of water vapor (ρ_{H2O}) and carbon dioxide (ρ_{CO2}) measured at a 10 Hz sampling rate. The observations between 2009 and 2012 were conducted by using a CSAT3 3-D sonic anemometer (Campbell Scientific, Inc., USA) and a LI-7500D open-path gas analyzer (LI-COR, USA) at 26 m above the surface level (a.s.l.). From 2013 to 2017, an IRGASON integrated sonic anemometer and open-path gas analyzer (Campbell Scientific, Inc., USA) operating at 25.4 m a.s.l. were used. According to Silveira et al. (2022), the turbulence measurement height at the PM IAG site was within the ISL, where the individual impacts of the elements in the RSL were negligible. To objectively assure that turbulence measurements were conducted in the ISL, a hypothesis testing was used by Silveira et al. (2022) to demonstrate that the coefficients of the similarity functions for normalized standard deviations of u, v, and w under neutral conditions found at the PM IAG were equal to Roth's (2000) averages, whose values are characteristic of an urban ISL (Barlow et al. 2014).

The footprint analysis by Silveira et al (2022) revealed that the source area contributing to 90% of the turbulent flux measurements at the PM IAG site in the period 2009–2017 lies within a 500 m radius from the tower. The source area extends mainly to the south-east and south (i.e., the prevailing wind directions), where vegetation coverage is greater (76% and 38%, respectively) (Fig. 1b, c). Consequently, flux measurements at the PM IAG site reveal

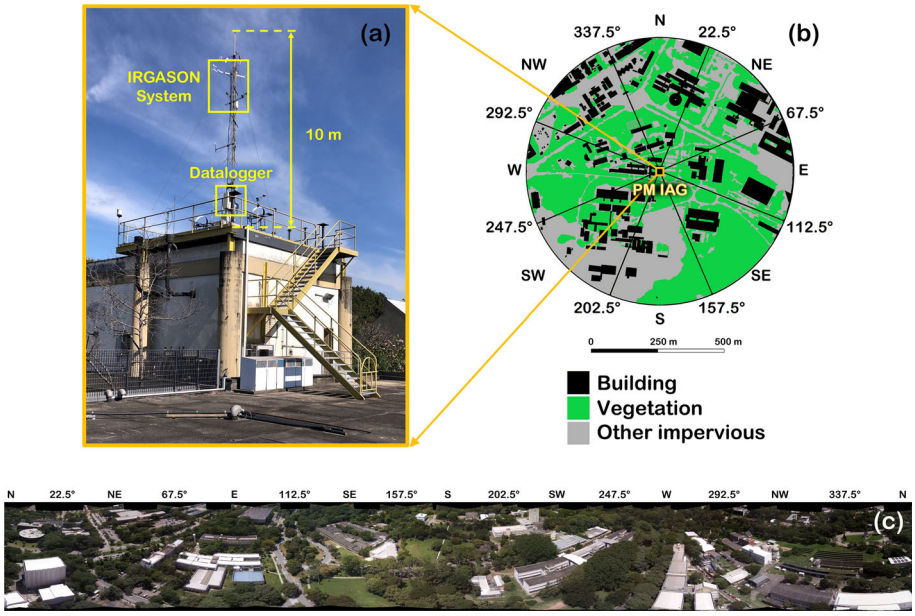

Fig. 1 Turbulence data acquisition system (**a**), land cover classification within a 500 m radius (**b**), and panoramic view (**c**) at the PM IAG site. In (**a**), a measurement system composed of an IRGASON integrated sonic anemometer and open-path gas analyzer and a CR5000 datalogger (Campbell Scientific, Inc., USA) was set up on a 10 m lattice tower. Photography looking south-west. In (**b**), 'other impervious' encompasses streets, parking lots, and other paved surfaces. The 500 m radius is centered at the PM IAG building. The various land cover types are distributed in geographical direction: north (N), north-east (NE), and subsequent directions. In (**c**), the photography was taken approximately 50 m above the surface, centered on the micrometeorological platform, and encompasses the land cover within the 500 m radius

characteristics similar to those of vegetated surfaces, as expected for suburban areas. For instance, Oliveira et al. (2020) verified positive CO_2 fluxes (emissions) during the night-time due to local vegetation respiration and negative CO_2 fluxes (absorption) during the daytime due to photosynthesis at the PM IAG in the summer of 2013. On the other hand, in the winter, the CO_2 fluxes were predominantly positive. The topography of a circular area with a radius of 500 m around the PM IAG site is quite gentle (Oliveira et al. 2020) and slopes from the south (782 m a.m.s.l.) to the north (718 m a.m.s.l.). Therefore, a surface variation of 64 m at a horizontal distance of 1 km can be presumed to minimally influence microscale features of the surface flow around the PM IAG site. As indicated by Fig. 1b, and discussed in the following paragraphs, the land use is the predominant factor in this case.

In terms of the local climate zone (LCZ), the PM IAG surrounding is classified as LCZ 6 (Oliveira et al. 2020). Generally, the land cover within a 500 m radius is composed of 18% buildings and 43% vegetation, while the remaining fraction consists of other impervious surfaces (paved streets, parking lots etc.) (Fig. 1b, c). The mean building height $\overline{H}$ is 6.6 m with a standard deviation σ_H of 4.7 m. According to Silveira et al. (2022), the mean tree height within the radius of 500 m could be estimated on the order of 10 m. For different geographical direction sectors, the building coverage ranges between 7% (south) and 24% (north), whereas the vegetation coverage ranges between 26% (south-west) and 76% (south-east). These surface heterogeneities impact the zero-plane displacement, d, and roughness length, z_0, whose values range from 13.9 m (south) to 16.6 m (west) and from 0.27 m

(south-west) to 0.60 m (south) (Silveira et al. 2022). The surface aerodynamic properties were estimated using anemometric methods for in situ turbulence measurement at a single level based on the temperature variance (Rotach 1994) and friction velocity (Toda and Sugita 2003). In this study, the variability of d was accounted for spectral analysis (see Sect. 2.2).

2.2 Data Processing

The spectra and cospectra were determined using the MBFLUX algorithm developed for turbulence data processing (Oliveira et al. 2020; Silveira et al. 2022). First, the 2009–2017 time series was partitioned into 30 min blocks based on the multiresolution flux decomposition (MRD) analysis used to determine the averaging timescale (Appendix 1). Thereafter, every block was subjected to data quality control (DQC), which included nonstationarity tests, flow distortion analysis, instrumental problem detection (spurious spikes, low signal strength etc.), Webb correction for water vapor and CO_2 density fluxes (Foken et al. 2012), and other procedures. Stationarity was assessed by using Vickers and Mahrt's (1997) and Mahrt's (1998) tests. These tests consist of the following parameters: (a) relative nonstationarity, RN_x, defined as the difference between the x values (given by linear regression) at the beginning and end of the block, normalized by the block average (for $x = u, v, w$); (b) wind speed reduction, defined as the ratio of the speed of the vector averaged wind to the averaged instantaneous speed; (c) nonstationarity ratio, NR, defined as the ratio of the standard deviation of the fluxes $\overline{(w'x')}_i$, derived from sub-blocks within the data block, to the standard deviation of the mean of fluxes $\overline{(w'x')}_j$ within each sub-block, averaged over all sub-blocks (for $x = u, T$ and $i, j = 1, \ldots, 6$). Nonstationary events were detected when $RN_x > 0.5$, $NR > 2$, or the wind speed reduction fall below 0.9. Flow distortions were detected through the analysis developed by Silveira et al. (2022) for neutral stability conditions. Basically, the test assesses the deviation of the normalized standard deviation of w from its urban mean of 1.25 (Roth 2000) within geographical direction bins of 22.5°. The comparison is made by hypothesis testing at a level of significance of 0.01. Bins with flow distortion are detected and removed when the deviations (or differences) are statistically significant.

The sonic anemometer tilt correction procedure consists of the planar fit method (Wilczak et al. 2001) used to align anemometer axes with the mean streamline coordinate system. This method removes the mean vertical velocity biases (offset error) and minimizes the over rotation risks since the resultant vertical axis is independent of the wind direction. In addition, it is suitable for tall vegetation and complex terrain (such as those found in suburban areas) (Rebmann et al. 2012).

The data number in the 30 min block was reduced to 2^{14} (~ 27.3 min) to apply a fast Fourier transform. The signal was conditioned through linear detrending and tapering with Hamming window (which decreases the amplitude of signal discontinuity at the beginning and end of the block) to remove noise in the low- and high-frequency ranges (Kaimal and Kristensen 1991; Fortuniak and Pawlak 2015). To avoid aliasing process, the cutoff frequency was defined as 5 Hz. The spectra and cospectra were smoothed by applying bin averages distributed across 30 normalized frequency bands of equal widths, on a logarithmic scale, within the range from 0.001 to 100 (cf. Kaimal and Gaymor 1983). The normalized frequency, $f = n(z - d)/\overline{U}$, where n is the natural frequency (in Hz), z is the measurement height a.s.l., and $\overline{U}$ is the mean wind speed at the z level, was estimated using the corresponding value of d from each geographical direction sector (see Sect. 2.1). This procedure avoids potentially

overestimated (or underestimated) values of f introduced by choosing a constant value for d in all geographical directions.

The resulting dataset used in the spectral analysis (see Sect. 3) encompasses 15,698 half-hour blocks (or 7,849 h) of turbulence measurements, corresponding to 20% of the original dataset. Nonstationarity events contribute significantly to the removal of raw data. In addition, the geographical direction sectors 67.5–135.0° and 292.5–337.5° were removed due to flow distortions caused by the tower blocking effect, as well as sensors themselves (e.g., gas analyzer close to the sonic paths), and updrafts over the PM IAG building, respectively (Fig. 1). Instrumental problems and other events were infrequent. A detailed description of the DQC was provided by Silveira et al. (2022).

2.3 Theoretical Framework

Kolmogorov's law predicts that the spectra of the wind velocity components and scalars, normalized by their characteristic scales x_*, are expressed in the inertial subrange by:

$$\frac{nS_x(n)}{x_*^2} = a_x F_x(\zeta') f^{b_x}, \tag{1}$$

where $F_x = \phi_\varepsilon^{2/3}$ for wind components ($x = u, v, w$) and $F_x = \phi_{N_x}\phi_\varepsilon^{-1/3}$ for scalars ($x = T$, ρ_{H2O}, ρ_{CO2}). ϕ_ε and ϕ_{N_x} are the normalized dissipation rates of TKE and half the variance of x, respectively. These normalized dissipation rates depend on the stability parameter $\zeta' = (z-d)/L$ given by the effective measurement height, z—d, and the Obukhov length, L. For wind velocity components, x_* is defined as the friction velocity $u_* = \left(\overline{u'w'}^2 + \overline{v'w'}^2\right)^{1/4}$ given by the vertical fluxes $\overline{u'w'}$ and $\overline{v'w'}$ of u and v components, respectively. With respect to the scalars, $x_* = -\overline{w'x'}/u_*$, where $\overline{w'x'}$ is the vertical flux of the scalar x. $a_x = \alpha_x/(2\pi\kappa)^{2/3}$, which depends on the von Kármán constant κ (here assumed to be equal to 0.40) and the Kolmogorov constant α_x for x, and $b_x = -2/3$.

Based on the local equilibrium hypothesis, observations in urban areas indicating unstable conditions $\phi_\varepsilon^{2/3}$ can be expressed as:

$$\phi_\varepsilon^{2/3}(\zeta') = \left[\phi_m(\zeta') - c_1\zeta'\right]^{2/3}, \tag{2}$$

where $\phi_m = \left(1 - c_2\zeta'\right)^{p_1}$ is the shear production and $\{c_1, c_2, p_1\}$ are empirical constants (Kanda et al. 2002; Roth et al. 2006; Fortuniak and Pawlak 2015). For stable conditions, Fortuniak and Pawlak (2015) verified that the normalized dissipation rate of TKE can be described by:

$$\phi_\varepsilon^{2/3}(\zeta') = 1 + c_3\zeta'^{3/5}. \tag{3}$$

This was proposed by Wyngaard and Coté (1971), within the stability range $0 < \zeta' < 0.5$. Several turbulence studies reported an imbalance between the production and dissipation terms of TKE (i.e., ϕ_m–$\phi_\varepsilon \neq 0$) under neutral conditions (e.g., Pahlow et al. 2001; Li et al. 2008; Babić and Rotach 2018). This imbalance is addressed by introducing an imbalance factor, $\phi_\varepsilon(0)$, defined by the ϕ_ε value for neutral conditions in (2)–(3).

Under stationary conditions, the normalized dissipation rate ϕ_{N_x} for scalar variances is usually taken as equal to the normalized production of half the temperature variance, ϕ_h, which has the form $\phi_h(\zeta') = \left(1 - c_4\zeta'\right)^{-1/2}$ for unstable conditions and $\phi_h(\zeta') = 1 + c_5\zeta'$

for stable conditions (Norman et al. 2012). Considering $\phi_{N_x} = \phi_h$, it is expected for unstable conditions that $F_x \longrightarrow 0$ as $\zeta' \longrightarrow$ -∞, whereas for stable ones $F_x \longrightarrow +\infty$ as $\zeta' \longrightarrow +\infty$. In addition, F_x tends to a constant value ($F_x \approx 1$) when $\zeta' \longrightarrow 0$. Therefore, based on the F_x behavior at different limits, its analytical form can be expressed for unstable and stable conditions respectively as:

$$F_x(\zeta') = (1 - c_6\zeta')^{-|p_2|}, \tag{4}$$

and:

$$F_x(\zeta') = 1 + c_7\zeta', \tag{5}$$

where $\{c_6, c_7, p_2\}$ are constants. The simple dependence of F_x on ζ' in Eq. (4) arises from the faster decay of ϕ_h, attributed to its -1/2 exponent, compared to the $\phi_\varepsilon^{-1/3}$ decay. As a result, the form of the similarity function of F_x is nearly identical to the ϕ_h function.

However, Roth et al. (2006) performed turbulence measurements above building roofs (i.e., on the top of the RSL) in Basel, CH, and their results indicated that under unstable conditions ϕ_{N_T} tends to increase as ζ' approaches zero, leading to higher values of F_T. For nearly neutral conditions, the surface heterogeneity increases the production of temperature variance when heat flux values are low (Tampieri et al. 2009). A similar result was found by Pahlow et al. (2001) for stable conditions in rural areas composed of different types of ground cover (heterogeneous). In addition, they also observed that ϕ_{N_T} tends to a constant value ($\phi_{N_T} \approx 1$) as the stability increase. Therefore, F_T must be expressed more adequately by:

$$F_T(\zeta') = c_8 + c_9|\zeta'|^{-|p_3|}, \tag{6}$$

for both stable and unstable conditions.

By extending the assumption of universal equilibrium theory to the normalized cospectra of the vertical fluxes of momentum and scalars, in the inertial subrange, these cospectra can be described by expressions of the form:

$$-\frac{nCo_{wx}(n)}{u_* x_*} = a_{wx} G_{wx}(\zeta') f^{b_{wx}}, \tag{7}$$

for $x = u,\ T,\ \rho_{H2O},\ \rho_{CO2}$. The parameters $a_{wx} = \alpha_{wx}/(2\pi\kappa)^{4/3}$ and $b_{wx} = -4/3$, where α_{wx} is a universal constant for covariance of w and x. G_{wx} expresses the product of $\phi_\varepsilon^{1/3}$ and the normalized vertical gradient of x (Roth and Oke 1993). For unstable conditions, G_{wx} is constant and equal to unity, whereas for stable conditions, follows the expression $G_{wx}(\zeta') = 1 + c_{wx}\zeta'$ proposed by Kaimal et al. (1972), where c_{wx} is an empirical constant. Fortuniak and Pawlak (2015) verified that for stable conditions, functions of the form:

$$G_{wx}(\zeta') = 1 + c_{wx}\zeta'^{|p_{wx}|}, \tag{8}$$

displayed the best fit to the average data of G_{uw} in Łódź, PL, and recommended caution only when defining the type of functional dependence between G_{wx} and ζ'. In the present study, Eq. (8) is used since it better describes the behavior of the data for São Paulo (see Sect. 3).

3 Results

3.1 Spectral Parameters in the Inertial Subrange

Coefficients $a_x F_x$ and b_x were estimated by fitting Eq. (1) to the spectrum of each 30 min block in the inertial subrange, defined here for $1 < f < 10$ based on the S_v/S_u results in Sect. 3.3, via the least squares method. Following the Fortuniak and Pawlak's (2015) criterion, only fit results that showed b_x deviates less than 8% from the expected value $-2/3$ were considered. For temperature spectra this deviation threshold was set as 200% to evaluate the divergence of the dissipation rate by Eq. (6) .

The coefficients b_x are close to the $-2/3$ power predicted by Kolmogorov's law as observed in other studies in (sub)urban areas (e.g., Roth and Oke 1993; Oikawa and Meng 1995; Roth et al. 2006; Christen et al. 2009; Fortuniak et al. 2015; Ramamurthy and Pardyjak 2015). In particular, the increase of the T spectra in the inertial subrange due to divergence of F_T under neutral conditions is on the order of $b_T = 0.44$. The coefficients $a_x F_x$ for neutral conditions, $a_u F_u(0) = 0.14$, $a_v F_v(0) = 0.20$, and $a_w F_w(0) = 0.24$, are less than the values found by Fortuniak and Pawlak (2015) in Łódź (0.310–0.320, 0.420–0.425, and 0.350–0.355, respectively) by a factor on the order of 1/2 for the u and v normalized spectra, whereas for w this factor is slightly lower (~ 2/3). Despite these differences, the $a_v F_v(0)/a_u F_u(0)$ ratio of 1.4 approaches the value 4/3 predicted by local isotropy with a difference of 5%, in agreement with Fortuniak and Pawlak (2015). On the other hand, the ratio $a_w F_w(0)/a_u F_u(0)$ of 1.7 is greater than that in other turbulence studies in urban areas where this ratio is typically less than 4/3 (e.g., Feigenwinter et al. 1999; Roth et al. 2006; Christen et al. 2009; Fortuniak and Pawlak 2015). This issue is discussed in the following sections.

3.2 Kolmogorov Constant

Several values of the Kolmogorov constant for the alongwind component, α_u, derived from atmospheric measurements, wind tunnels etc., have been reported in the literature ranging from 0.36 to 0.59 (Dyer and Hicks 1982; Högström et al. 1990; Cheng et al. 2010). The value proposed for α_u by Högström (1990) and posteriorly developed by Högström et al. (1996) of 0.52 has been used in turbulence studies (e.g., Nilsson et al. 2016; Hackerott et al. 2017; Andersson et al. 2019; Roy et al. 2021). Due to local isotropy, α_v and α_w are expected to both equal 4/3 α_u (Fortuniak and Pawlak 2015). Hence, the Kolmogorov constant for v and w can be evaluated as 0.69 for $\alpha_u = 0.52$.

By setting $F_x(0) = 1$ based on the local equilibrium hypothesis, the Kolmogorov constant for the wind component x can be estimated through the median of the coefficients $a_x F_x$ under neutral conditions. Following this methodology, the value of α_u obtained in this study, 0.26, is less than those found in the literature. Similarly, the values of α_v (0.37) and α_w (0.45) are also less than the expected value (~ 0.69), although they are close to the estimates of 0.48 and 0.50, respectively, obtained by Kaimal et al. (1972) who performed turbulence measurements on quasi-ideal surface (Table 1).

The differences greater than 27% observed between the α_u values from this study and those reported in the literature indicate a possible imbalance between local production and dissipation terms of TKE. According to Högström (1990), the imbalance factor can be expressed as $\phi_\varepsilon(0) = (0.26/0.52)^{3/2} \approx 0.35$, where 0.52 was assumed to be the reference value for α_u. This result shows an 'inadequate dissipation' of turbulence (Li et al. 2008) since only 35% of the TKE yielded is locally dissipated under neutral conditions. Note that $[\phi_\varepsilon(0)]^{2/3} \approx 0.50$,

Table 1 Coefficients fitted to the normalized (co)spectra under neutral conditions

x	Spectrum				
	$a_x F_x(0)$	b_x	α_x	$F_x(0)$	m
u	0.14 ± 0.04	-0.65 ± 0.03	0.26 ± 0.08	0.50	875
v	0.20 ± 0.05	-0.65 ± 0.04	0.37 ± 0.10	0.53	821
w	0.24 ± 0.08	-0.65 ± 0.03	0.45 ± 0.15	0.65	648
T	0.6 ± 0.5	$+0.44 \pm 0.21$	1.2 ± 1.0	1.5	1033
ρ_{H2O}	0.21 ± 0.12	-0.65 ± 0.04	0.38 ± 0.22	0.48	184
ρ_{CO2}	0.26 ± 0.16	-0.65 ± 0.03	0.5 ± 0.4	0.6	179
wx	Cospectrum				
	$a_{wx} G_{wx}(0)$	b_{wx}	α_{wx}	$G_{wx}(0)$	m
uw	0.043 ± 0.025	-1.32 ± 0.08	0.15 ± 0.09	0.38	111
wT	0.08 ± 0.03	-1.32 ± 0.06	0.26 ± 0.12	0.65	292
$w\rho_{H2O}$	0.07 ± 0.03	-1.32 ± 0.07	0.24 ± 0.11	0.60	222
$w\rho_{CO2}$	0.07 ± 0.03	-1.32 ± 0.08	0.25 ± 0.12	0.62	179

The values are presented as the medians ± median absolute deviations. Neutral conditions were defined for $|\zeta| < 0.01$ m is the number of 30 min blocks. $F_x = \phi_\varepsilon^{2/3}$ (for $x = u, v, w$) and $F_x = \phi_{N_x} \phi_\varepsilon^{-1/3}$ (for $x = T$, ρ_{H2O}, ρ_{CO2}), where ϕ_ε and ϕ_{N_x} are the normalized dissipation rates of turbulent kinetic energy and half the variance of x, respectively. G_{wx} is the normalized dissipation rate of the vertical flux of x. $F_x(0)$ and $G_{wx}(0)$ are imbalance factors of the dissipation rates given by the ratio α_x/α_{ref}, where the reference values of the Kolmogorov constants were defined as $\alpha_{ref} = 0.52$, 0.80, and 0.40 for velocity, scalar, and flux, respectively. α_x is the Kolmogorov constant for x, and α_{wx} is the universal constant for the w and x cospectrum assuming $F_x(0) = G_{wx}(0) = 1$

which could explain why the $a_x \phi_\varepsilon^{2/3}(0)$ estimates are on the order of half the values found by Fortuniak and Pawlak (2015). Other studies in urban areas have also reported inadequate dissipation of TKE under near neutral conditions (Clarke et al. 1982; Roth and Oke 1993; Kanda et al. 2002; Roth et al. 2006), as well as in rural areas and on an extensive plain of tall dry grass (e.g., Oncley et al. 1996; Pahlow et al. 2001; Li et al. 2008; Frenzel and Vogel 2001). Li et al. (2008) concluded that this imbalance was associated with the vertical transport of turbulence to upper layers due to the pressure and TKE transport terms. In addition, as noted by Roth and Oke (1993), in an urban environment, the interaction between flow and roughness elements, added to other factors (e.g., plumes), could increase the transport of local TKE, as well as scalar variance, to the atmosphere, leading to inadequate dissipation. On the other hand, Fortuniak and Pawlak (2015) verified an excess of local dissipation at urban sites (i.e., $\phi_\varepsilon(0) > 1$), showing a dissipation up to 21% greater than the local production, similar to the rural area results from Högström et al. (1990). Despite the observed imbalance, Fortuniak and Pawlak (2015) verified that similarity functions (2)–(3) based on the local equilibrium hypothesis could be applied in urban areas and confirmed the close relationship between ϕ_ε and ϕ_m.

With respect to the scalars, the value of the Kolmogorov constant for CO_2 density of (0.6) agrees with the value of 0.68 estimated by Norman et al. (2012) through turbulence measurements at a land-based marine station in the Baltic Sea. However, both values are

less than the estimates derived from the measurements over sea, plantations, and grass land, which vary between 0.78 and 0.89 (Ohtaki 1982; Verma and Anderson 1984; Iwata et al. 2005; Cheng et al. 2010). Similarly, the Kolmogorov constant for water vapor density also has a value (0.47) less than the estimates reported in the literature, such as the value of 0.76 obtained by Iwata et al. (2005) or 0.99 by Verma and Anderson (1984). Despite these differences, the $\alpha_{\rho_{\mathrm{H2O}}}$ determined in this study is comparable to the value of 0.58 estimated by Smedman-Högström (1973) in rural area. On the other hand, the α_T is greater than the value of 0.80 proposed by Högström (1996) due to the divergence of F_T observed for neutral conditions in urban areas.

As observed for wind components, the possibly underestimated values for the Kolmogorov constants $\alpha_{\rho_{\mathrm{H2O}}}$ and $\alpha_{\rho_{\mathrm{CO2}}}$ may be associated with the imbalance between local dissipation and production of variance of ρ_{H2O} and ρ_{CO2}, because the common assumption that transport terms are negligible (or equal in magnitude) is not always valid (Sjöblom and Smedman 2002; 2004). For instance, by assuming the hypothesis $\alpha_T = \alpha_{\rho_{\mathrm{H2O}}} = \alpha_{\rho_{\mathrm{CO2}}} \approx 0.80$ based on results from Andreas (1987), Iwata et al. (2005), and Cheng et al. (2010), and that $\phi_\varepsilon(0) = 0.35$ for the present site, the imbalance factor for scalars can be evaluated as $\phi_{N_x}(0) \approx \alpha_x / 0.80 \times 0.35^{1/3}$ based on the procedure developed for $\phi_\varepsilon(0)$ (see Högström 1990). Hence, only 53% and 41% of the locally yielded variance of ρ_{H2O} and ρ_{CO2} would have been dissipated, respectively. In particular, the local dissipation of temperature variance would have been on the order of the local production.

3.3 Isotropic Ratio

In the inertial subrange, where TKE transfer from large to small scales occurs, if the turbulence is locally isotropic such that the statistical properties of the velocity field are independent of the rotation and reflection in the coordinate system, then the spectral roll-off is expected to follow the $-2/3$ power law, and the spectral ratios S_v/S_u and S_w/S_u tend to the 4/3 ratio (Kolmogorov 1991). The S_v/S_u (S_w/S_u) values were estimated by dividing the median of the v (w) normalized spectra by the median of the u normalized spectra for each frequency band under different stability condition. Our results indicate that the spectral ratios tend to a constant value in the frequency range given by $f = 1$–10 and they converge to the 4/3 isotropic ratio under near-neutral conditions (at least for S_v/S_u) (Fig. 2). These results agree with the frequency range observed in other studies (e.g., Roth 2000; Roth et al. 2006; Fortuniak and Pawlak 2015). Under neutral conditions, defined for $\left|\zeta'\right| < 0.01$, the S_v/S_u and S_w/S_u values in the range $1 < f < 10$ are on the order of 1.4 and 1.7, respectively. S_v/S_u values between 1.3 and 1.5 were reported over (sub)urban surfaces (Lundquist et al. 2004; Fortuniak and Pawlak 2015), whereas considerable deviations from the classical theory of isotropy were observed for S_w/S_u within the RSL and above it in the ISL. Urban turbulence studies have shown values of S_w/S_u ranging from 0.8 to 1.3 (Roth and Oke 1993; Feigenwinter et al. 1999; Roth 2000; Lundquist et al. 2004; Roth et al. 2006; Fortuniak and Pawlak 2015).

3.3.1 Taylor's Hypothesis Violation

Roth et al. (2006) reasoned that a possible explanation for the deviation in urban environments of S_w/S_u from the predicted value was Taylor's hypothesis violation. This hypothesis suggests that all turbulent eddies are advected in the mean wind direction without changes in their properties (Cheng et al. 2017). The Taylor's hypothesis is expected to hold for turbulent intensities $\sigma_u/\overline{U}$ less than 0.5, where σ_u is the standard deviation of u (Willis and Deardorff

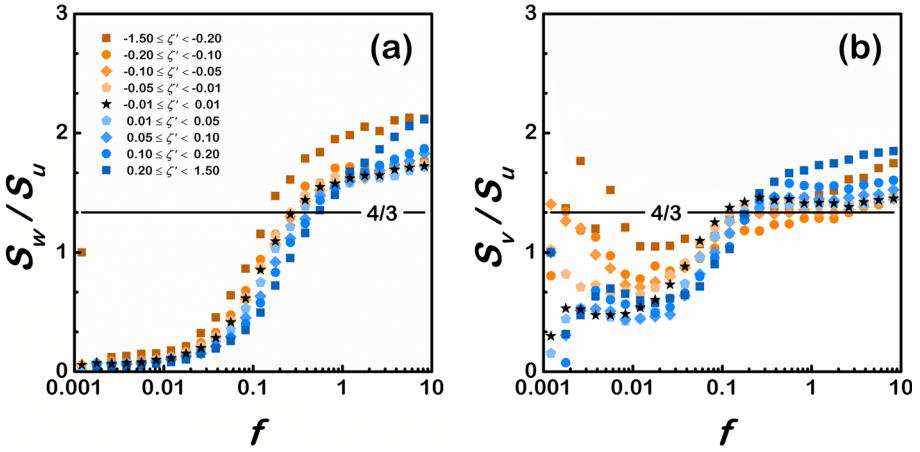

Fig. 2 Spectral densities of the (**a**) vertical and (**b**) lateral velocity components (S_w and S_v respectively) relative to the longitudinal velocity spectrum (S_u) for different stability subranges. ζ' is the stability parameter and f is the normalized frequency. Unstable (stable) conditions are indicated by orange (blue) shading and neutral conditions are indicated by black stars. The black solid line indicates the 4/3 value predicted by isotropy (Kolmogorov 1991)

1976). In this study, however, only 3% of data exceeded this threshold. In addition, the results did not change when constraining the data only to conditions where $\sigma_u/\overline{U} < 0.5$ (not shown). This implies that the S_w/S_u deviation from the 4/3 ratio in the inertial subrange is due to a factor other than the Taylor's hypothesis violation.

3.3.2 Local Imbalance of TKE

Stiperski et al. (2019) verified that over complex surfaces (e.g., sloped, horizontally heterogeneous, and aerodynamically rough), the turbulence complexity, defined by the departure of the turbulent structure from its 'canonical form' over ideal surfaces, could be related with how much the ratios of dissipation rates for velocity components in the inertial subrange, $\varepsilon_v/\varepsilon_u$ and $\varepsilon_w/\varepsilon_u$, deviate from unity. Under neutral conditions, these ratios can be expressed as $\varepsilon_v/\varepsilon_u = [3a_v F_v(0)/4a_u F_u(0)]^{3/2}$ and $\varepsilon_w/\varepsilon_u = [3a_w F_w(0)/4a_u F_u(0)]^{3/2}$.

In this study, the ratio $\varepsilon_v/\varepsilon_u$ of the horizontal components was of 1.1. In contrast, $\varepsilon_w/\varepsilon_u$ was of 1.5, indicating that the normalized dissipation rate of TKE in the w direction was greater than in u direction. Similar behavior can be verified for the $a_x F_x(0)$ coefficients obtained by Fortuniak and Pawlak (2015) in the ISL, whose ratios of the horizontal components were on the order of one, whereas the $\varepsilon_w/\varepsilon_u$ values also deviated from unity. However, their ratios indicated that the dissipation rate in the w direction was less than in the u direction in Łódź. These results could explain why S_v/S_u and S_w/S_u are higher or lower than the expected value of 4/3 in urban areas (e.g., Lundquist et al. 2004; Roth et al. 2006; Fortuniak and Pawlak 2015). In addition, they suggest that the spectral ratio departure may be related with the local imbalance between the dissipation and production of TKE in the velocity component directions. Indeed, Babić and Rotach (2018) verified that over heterogeneous surfaces the TKE dissipation rates are not the same in all three directions.

According to Li et al. (2008), an inadequate or excess TKE dissipation is characterized by values of $\phi_\varepsilon(0)$ less or greater than the unity, respectively. In the present site, only 35% of the

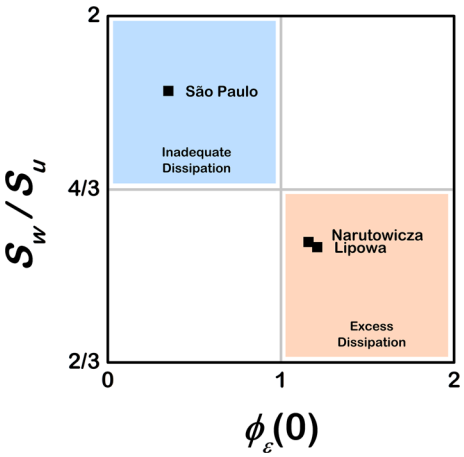

Fig. 3 Quadrant analysis of the relation between the spectral ratio S_w/S_u and dissipation rate of TKE under neutral conditions. The data (São Paulo) in the 2nd quadrant (blue) are characterized by inadequate TKE dissipation, while in the 4th quadrant (orange) by excess dissipation. Lipowa and Narutowicza correspond to the urban data from Fortuniak and Pawlak (2015)

local production of TKE is dissipated (see Sect. 3.2). In Łódź, Fortuniak and Pawlak (2015) found dissipation exceeding local production between 16 and 21%. These results indicate that S_w/S_u tend to increase under conditions of inadequate TKE dissipation and decrease for excess dissipation, as showed in Fig. 3. However, this hypothesis needs to be more thorough investigated in future studies of turbulence over urban surfaces. To the best of the authors' knowledge, no other urban study has both parameters S_w/S_u and $\phi_\varepsilon(0)$ to draw more accurate conclusions.

3.4 Cospectral Parameters and the Universal Constant

By submitting the coefficients $a_{wx}G_{wx}$ and b_{wx} to a procedure analogous to that used for spectra, were obtained b_{wx} values close to the $-4/3$ power law at the inertial subrange (Table 1). The value of 0.06 for $a_{uw}G_{uw}$ under neutral conditions agrees with the value of 0.07 found by Fortuniak and Pawlak (2015) in their urban sites. For scalar fluxes, $a_{wx}G_{wx}(0)$ is on the order of 0.07. This result suggests that $a_{wT}G_{wT}(0) \approx a_{w\rho_{H2O}}G_{w\rho_{H2O}}(0) \approx a_{w\rho_{CO2}}G_{w\rho_{CO2}}(0)$. Su et al. (2004) found values for $a_{wT}G_{wT}(0)$ greater than for São Paulo (0.090–0.160) based on turbulence measurements over forests. In addition, Su et al. (2004) verified that $a_{wT}G_{wT}(0)$ varied with the measurement height, season, and canopy morphology. This indicates that the $a_{wx}G_{wx}$ values found in São Paulo for the scalar fluxes may diverge from those in other urban sites.

By assuming $G_{wT}(0) = G_{w\rho_{H2O}}(0) = G_{w\rho_{CO2}}(0) = 1$, the Kolmogorov constant for the scalar fluxes in this study range from 0.24 to 0.26 (Table 1). These results are up to 40% less than the value of 0.40 estimated for α_{wT} over flat and homogeneous surface (Kaimal et al. 1972; Wyngaard and Coté 1972). The differences between these estimates are probably due to the imbalance observed for ϕ_ε under neutral conditions. For example, $G_{wT}(0) \approx [\phi_\varepsilon(0)]^{1/3} \approx 0.35^{1/3} \approx 0.70$. Hence, when the imbalance effect is corrected, $a_{wT} = 0.08/G_{wT}(0) \approx 0.08/0.70 \approx 0.11$ and approaches to the value of $1.6/(2\pi)^{4/3}$ reported for a_{wT} by Kaimal et al. (1972) and Wyngaard and Coté (1972). In addition, the Kolmogorov constants found for the scalar cospectra suggest that $\alpha_{wT} = \alpha_{w\rho_{H2O}} = \alpha_{w\rho_{CO2}}$.

3.5 Normalized Dissipation Rates of Variances

Equations (2)–(6) were fitted to the bin medians of $a_x\phi_\varepsilon^{2/3}$, $a_x F_x$ (for $x = \rho_{CO2}, \rho_{H2O}$), and $a_T F_T$, respectively. These medians correspond to the stability bins of equal width, logarithmically distributed, and represent a more robust measure of the central tendency. A constraint of at least 10 data points per bin was defined to ensure a minimum statistical representativeness. The weighted least squares (WLS) method was used in the regressions to ensure the most precise parameter estimates, where the weights were set as the inverse of the interquartile range (IQR) of each bin. The IQR is the central 50% of the data and is defined as the difference between the 75th and 25th percentiles. As imposed in Sect. 3.1, only fit results that showed spectral slopes that deviate less than 8% from the theoretical − 2/3 slope were considered in the analysis. The inertial subrange was defined as $1 < f < 10$.

By considering a_x to be independent of stability (Su et al. 2004), the similarity functions for normalized dissipation rates were determined through the ratio between the coefficients and their mean values for neutral conditions ($|\zeta'| < 0.01$) to remove the imbalance effect, with the exception of $a_T F_T$. The $a_T F_T$ values were divided by $\alpha_T/(2\pi\kappa)^{2/3}$ (where α_T was defined as 0.8) due to F_T divergence under neutral conditions (Fig. 4). Based on the results for urban areas (e.g., Kanda et al. 2002; Roth et al. 2006) the similarity function of normalized shear production was defined as $\phi_m(\zeta') = \left(1 - c_2\zeta'\right)^{-1}$ for unstable conditions. Following Fortuniak and Pawlak's (2015) methodology, the behavior of the normalized dissipation rate of TKE was analyzed by fitting (2)–(3) to the bin medians encompassing all velocity component data together and separately in the u, v, and w directions (see Appendix 2) to determine more statistically reliable results. The goodness of fit was assessed through

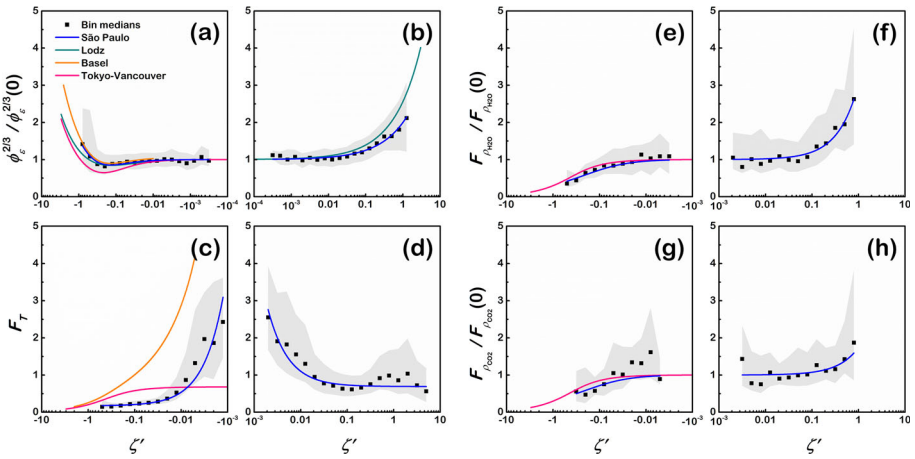

Fig. 4 Normalized dissipation rates of (**a–b**) turbulent kinetic energy and (**c–h**) half the scalar variance. $F_x = \phi_\varepsilon^{2/3}$ (for $x = u, v, w$) and $F_x = \phi_{N_x}\phi_\varepsilon^{-1/3}$ (for $x = T, \rho_{H2O}, \rho_{CO2}$), where ϕ_ε and ϕ_{N_x} are the normalized dissipation rates of turbulent kinetic energy and half the variance of x, respectively. $F_x(0)$ is the imbalance factor. ζ' is the stability parameter. In c–d the function F_T was not divided by its imbalance factor due to divergence of the data for neutral conditions. In e and g, the Tokyo-Vancouver curve is the product of the ϕ_{N_T} and $\phi_\varepsilon^{-1/3}$ functions obtained by Kanda et al. (2002) divided by their values at $\zeta' = 0$. The black squares and grey shading indicate the median and range between the 25th and 75th percentiles of the bins, respectively. Table 2 shows the similarity curves for São Paulo and other cities

the adjusted R-squared, R^2_{adj}, that accounts for the sample size and the degree of freedom, avoiding overestimated coefficients of determination for large samples.

Generally, the most values of R^2_{adj} were greater than 0.75 and indicate good representativeness of the data by the similarity functions (2)–(6) (Table 2). The smallest values were found for $F_{\rho_{CO2}}$ under unstable ($R^2_{adj} = 0.55$) and stable conditions ($R^2_{adj} = 0.42$), which were associated with the largest data dispersion in near neutral conditions (Fig. 4g, h). In addition, the fitting results demonstrate that the normalized dissipation rates of TKE and density variance of the passive gases divided by their neutral condition values can be described in urban areas by similarity functions based on the local equilibrium hypothesis (i.e., local dissipation equal to local production), and the Fortuniak and Pawlak's (2015) conclusions can also be extended to scalar variances.

Under unstable conditions, the similarity functions for $\phi_\varepsilon^{2/3}$ found in other cities underestimate the behavior of the data from São Paulo, which are described by $\phi_\varepsilon^{2/3}(\zeta') = [(1–6.2\ \zeta')^{-1}—1.80\ \zeta']^{2/3}$ (Fig. 4a; Table 2). In particular, the similarity function for Basel by Roth et al. (2006) shows less divergence than the functions from the other urban studies (e.g., Kanda et al. 2002; Fortuniak and Pawlak 2015). Under stable conditions, the function $\phi_\varepsilon^{2/3}(\zeta') = 1 + 1.56\ \zeta'^{3/5}$ found by Fortuniak and Pawlak (2015) in Łódź effectively describes the values of $\phi_\varepsilon^{2/3}$. However, this function tends to overestimate the values when $\zeta' > 0.1$. The best fit for stable conditions was obtained with the function $\phi_\varepsilon^{2/3}(\zeta') = 1 + 1.00\ \zeta'^{3/5}$ (Fig. 4b).

The similarity functions for F_T found by Kanda et al. (2002) and Roth et al. (2006) under unstable conditions do not describe the data divergence to $+\infty$ as ζ' approaches zero. Equation (6) represents the median behavior of F_T in urban areas more adequately (Fig. 4c). In this study, $F_T(\zeta') = 0.169 + 0.0037\ (-\zeta')^{-1}$ and $F_T(\zeta') = 0.69 + 0.0041\ \zeta'^{-1}$ were the best fits for unstable and stable conditions, respectively. Despite the F_T dispersion for $\zeta' > 1$, the mean values oscillate around a constant value given by the horizontal asymptote of 0.69, in agreement with the rural area results from Pahlow et al. (2001). The small fraction of F_T data for more unstable conditions ($\zeta' < -1$) is due to the nonstationary data removed during the post-processing procedures (see Sect. 2.2).

In contrast to F_T, under stable conditions, the values of $F_{\rho_{H2O}}$ and $F_{\rho_{CO2}}$ increase as the stability increases, described by the functions $F_{\rho_{H2O}}(\zeta') = 1 + 2.04\ \zeta'$ and $F_{\rho_{CO2}}(\zeta') = 1 + 0.74\ \zeta'$. On the other hand, similar to F_T, under unstable conditions, $F_{\rho_{H2O}}$ and $F_{\rho_{CO2}}$ medians decrease as instability increases. The best fit was obtained by the following functions: $F_{\rho_{H2O}}(\zeta') = (1–9\ \zeta')^{-1/2}$ and $F_{\rho_{CO2}}(\zeta') = (1–10\ \zeta')^{-1/2}$. These results indicate that $F_{\rho_{H2O}} \approx F_{\rho_{CO2}}$ in urban areas, as verified in turbulence studies conducted over sea and plantations under unstable conditions (e.g., Ohtaki 1982; Iwata et al. 2005). To the best of our knowledge, no similarity functions have been derived from urban areas for normalized dissipation rates of ρ_{H2O} and ρ_{CO2} variances in the literature. However, by assuming $F_{\rho_{H2O}} = F_{\rho_{CO2}} = F_T$, the behavior of $F_{\rho_{H2O}}$ and $F_{\rho_{CO2}}$ can be reasonably described by the expression found by Kanda et al. (2002) for F_T (using turbulence measurements in Tokyo, JP, and Vancouver, CA) when divided by its value at $\zeta' = 0$ (Fig. 4e, g). Note that both $F_{\rho_{H2O}}$ and $F_{\rho_{CO2}}$ decay with an exponent of $-1/2$. From this result, F_x can be presumed to be on the order of ϕ_{N_x}, as predicted in Sect. 2.3, since the normalized dissipation rate of variance ϕ_{N_x} also decays with an exponent of $-1/2$ under unstable conditions, as reported by several studies (e.g., Ohtaki 1982; Dyer and Bradley 1982; Högström 1988; Kanda et al. 2002; Iwata et al. 2005; Roth et al. 2006).

Table 2 Similarity functions of the normalized dissipation rates for urban areas

Normalized dissipation rates of variances				
	Unstable conditions $\phi_\varepsilon^{2/3}$	$F_{\rho_{H_2O}}$	$F_{\rho_{CO_2}}$	F_T*
São Paulo	$\left[(1-6.2\zeta')^{-1}-1.80\zeta'\right]^{2/3}$	$(1-9\zeta')^{-1/2}$	$(1-10\zeta')^{-1/2}$	$0.169+0.0037(-\zeta')^{-1}$*
	$R^2_{adj}=0.94$	$R^2_{adj}=0.91$	$R^2_{adj}=0.55$	$R^2_{adj}=0.89$
u component	$\left[(1-5.9\zeta')^{-1}-1.19\zeta'\right]^{2/3}$			
	$R^2_{adj}=0.70$			
v component	$\left[(1-11\zeta')^{-1}-3.03\zeta'\right]^{2/3}$			
	$R^2_{adj}=0.84$			
w component	$\left[(1-6\zeta')^{-1}-2.61\zeta'\right]^{2/3}$			
	$R^2_{adj}=0.86$			
Łódź[a]	$\left[(1-37\zeta')^{-1/4}-\zeta'\right]^{2/3}$	–	–	–
Basel[b]	$\left[(0.93-5.4\zeta')^{-1.1}-2\zeta'\right]^{2/3}$*	–	–	$1.42(-0.03-24\zeta')^{-0.46}\left[(0.93-5.4\zeta')^{-1.1}-2\zeta'\right]^{-1/3}$*
Tokyo-Vancouver[c]	$\left[(1-10.5\zeta')^{-1}-\zeta'\right]^{2/3}$	–	–	$0.68(1-9.69\zeta')^{-1/2}\left[(1-10.5\zeta')^{-1}-\zeta'\right]^{-1/3}$*

Table 2 (continued)

Normalized dissipation rates of variances				
	Unstable conditions			
	$\phi_\varepsilon^{2/3}$	$F_{\rho_{H_2O}}$	$F_{\rho_{CO_2}}$	$\boldsymbol{F_T}^*$
	Stable conditions			
	$\boldsymbol{\phi_\varepsilon}^{2/3}$	$F_{\rho_{H_2O}}$	$F_{\rho_{CO_2}}$	$\boldsymbol{F_T}$
São Paulo	$1 + 1.00\boldsymbol{\zeta}'^{3/5}$	$1 + 2.04\boldsymbol{\zeta}'$	$1 + 0.74\boldsymbol{\zeta}'$	$0.69 + 0.0041\boldsymbol{\zeta}'^{-1}$*
	$R^2_{adj} = 0.78$	$R^2_{adj} = 0.87$	$R^2_{adj} = 0.42$	$R^2_{adj} = 0.76$
$\boldsymbol{u}$ component	$1 + 0.82\boldsymbol{\zeta}'^{3/5}$			
	$R^2_{adj} = 0.81$			
$\boldsymbol{v}$ component	$1 + 1.30\zeta'^{3/5}$			
	$R^2_{adj} = 0.89$			
$\boldsymbol{w}$ component	$1 + 0.91\boldsymbol{\zeta}'^{3/5}$			
	$R^2_{adj} = 0.82$			
Łódź[a]	$1 + 1.56\boldsymbol{\zeta}'^{3/5}$	–	–	–

Table 2 (continued)

Normalized dissipation rates of fluxes				
	Unstable conditions			
	G_{uw}	$G_{w\rho_{H2O}}$	$G_{w\rho_{CO2}}$	G_{wT}
São Paulo	1.0 ± 0.8**	1.0 ± 0.7**	1.0 ± 0.6**	0.9 ± 0.5**
Vancouver[d]	–	< 1	–	< 1
	Stable conditions			
	G_{uw}	$G_{w\rho_{H2O}}$	$G_{w\rho_{CO2}}$	G_{wT}
São Paulo	$1 + 3.7\ \zeta'^{0.78}$	$1 + 2.3\ \zeta'^{0.65}$	$1 + 1.5\ \zeta'^{0.55}$	$1 + 1.55\ \zeta'^{0.42}$
	$R^2_{adj} = 0.94$	$R^2_{adj} = 0.91$	$R^2_{adj} = 0.66$	$R^2_{adj} = 0.89$
Łódź-Lipowa[a]	$1 + 3.3\ \zeta'^{0.57}$	–	–	–
Łódź-Narutowicza[a]	$1 + 5.8\ \zeta'^{0.68}$	–	–	–

$F_x = \phi_{N_x} \phi_\varepsilon^{-1/3}$, where ϕ_ε and ϕ_{N_x} are similarity functions of the normalized dissipation rates of turbulent kinetic energy and half the variance of x, respectively; R^2_{adj} is the adjusted R-squared; and nS_x/x_*^2 is the normalized spectrum of x

* Without imbalance effect correction
** Median ± Interquartile range
[a] Fortuniak and Pawlak (2013)
[b] Roth et al. (2006)
[c] Kanda et al. (2002)
[d] Roth and Oke (1993)

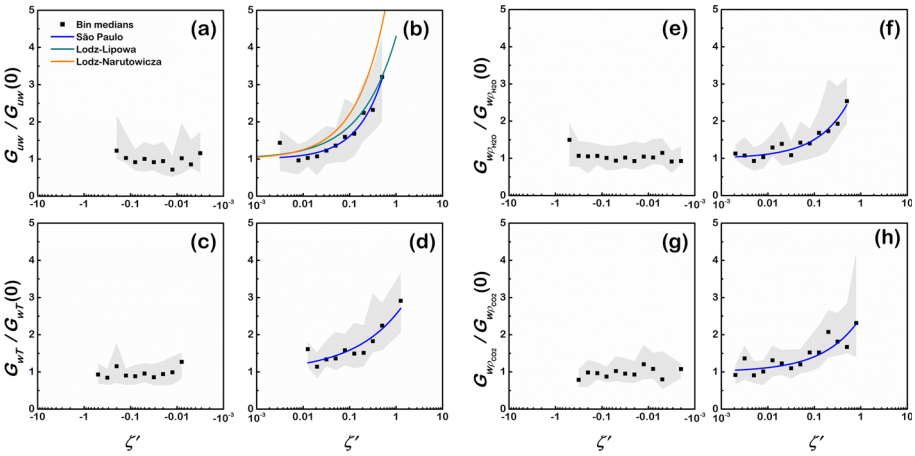

Fig. 5 Normalized dissipation rates of (**a–b**) momentum and (**c–h**) scalar fluxes. G_{wx} is the normalized dissipation rate of the vertical flux of x (for $x = u$, T, ρ_{H2O}, ρ_{CO2}). ζ' is the stability parameter. $G_{wx}(0)$ is the imbalance factor. The black squares and grey shading indicate the median and range between the 25th and 75th percentiles of the bins, respectively. Table 2 shows the similarity curves for São Paulo and other cities

3.6 Normalized Dissipation Rates of Fluxes

The similarity functions for G_{wx} were determined analogously to the normalized dissipation rates of TKE and scalar variance (see Sect. 3.5). The regression parameters were determined through the WLS method. By assuming that a_{wx} does not change with stability, the coefficients $a_{wx}G_{wx}$ were divided by their mean value under neutral conditions, $a_{wx}G_{wx}(0)$, to correct for the imbalance effect. Under unstable conditions, G_{wx} is nearly constant value, in accordance with the urban area results for momentum, heat, and humidity fluxes (Roth and Oke 1993; Fortuniak and Pawlak 2015) (Fig. 5a, c, e, g). The medians range from 0.9 to 1.0, in agreement with the value (equal to unity) predicted by Kaimal et al. (1972) (Table 2). In contrast, Roth and Oke (1993) verified that the values for G_{wT} and $G_{w\rho_{H2O}}$ in Vancouver were less than expected. Under stable conditions, the linear relationship given by Eq. (8) effectively described the data from São Paulo, which had R^2_{adj} values ranging from 0.65 to 0.94 (Fig. 5b, d, f, h; Table 2). In particular, Fortuniak and Pawlak's (2015) curves obtained in Łódź overestimated the behavior of G_{uw} data from São Paulo, which were better described by $G_{uw}(\zeta') = 1 + 3.7\ \zeta'^{0.78}$ for stable conditions. The following empirical constants were found for the scalar fluxes: $c_{wT} = 1.55$, $c_{w\rho_{H2O}} = 2.3$, and $c_{w\rho_{CO2}} = 1.5$. In particular, both exponents $p_{w\rho_{H2O}}$ and $p_{w\rho_{CO2}}$ are on the order of 0.6.

3.7 Normalized Spectra

By dividing the normalized spectra of wind components and scalars by the similarity functions F_x found in São Paulo, the dependence on ζ' can be removed, and the spectra of different stability conditions are expected to converge to a single straight line in the inertial subrange. Following Babić and Rotach (2018), the functions for the normalized TKE dissipation rate in the u, v, and w directions were determined to account for in the subsequent analysis the inadequate dissipation of the individual velocity components (Appendix 2, Sect. 3.3.2). To

analyze spectral evolution the stability parameter was distributed into 9 stability subranges within the range $-1.5 \leq \zeta' < 1.5$ (see Fig. 6). In this study, spectra under neutral conditions were defined in the stability subrange $-0.01 \leq \zeta' < 0.01$ based on the continuous transition of the spectrum from stable to unstable (Fortuniak and Pawlak 2015).

The normalized spectra for São Paulo converge in the inertial subrange, $1 < f < 10$, where the spectral intensity follows the Kolmogorov law and decays with an exponent on the order of $-2/3$ (see Table 1) as observed in other urban-area studies (e.g., Roth et al. 2003; Roth et al. 2006; Ramamurthy and Pardyjak 2015; Fortuniak and Pawlak 2015). The spectral peak of the wind components and temperature shows a dependence on ζ' by shifting to higher frequencies as the stability increases. This dependence is not clear for the ρ_{H2O} and ρ_{CO2} spectra, which display a 'minor peak' between $0.004 < f < 0.008$ for some stability subranges (Fig. 6e, f). This issue is further discussed below.

Under neutral conditions, the normalized spectrum across the entire frequency range can be described by boundary-layer models (Larsén et al. 2021). The Kaimal model is typically used in describing temperature and horizontal-wind components, displaying the following general form:

$$\frac{nS_x(n)}{x_*^2 F_x(0)} = \frac{c_{10} f}{(1 + c_{11} f^{p_4})^{p_5}}, \tag{9}$$

where $\{c_{10}, c_{11}\}$ are empirical constants, $F_x(0)$ is the imbalance factor (see Table 1), $p_4 = 1$, and $p_5 = 5/3$ (Kaimal et al. 1972). Fortuniak and Pawlak (2015) verified that the spectrum of the wind components was better described by defining $p_4 = 5/3$ and $p_5 = 1$ in Łódź. However, data from São Paulo show that the analytical form $nS_x(n)/x_*^2 F_x(0) = c_{10} f/(1 + c_{11} f)^{5/3}$ is more suitable for describing normalized spectra of velocity and scalars (Fig. 7a, b). The goodness of fit was assessed through the parameter R^2_{adj}, whose values varied from 0.89 to 0.99 (Table 3). The R^2_{adj} values indicated the lowest value for the T spectrum and is due to spectral increasing in the inertial subrange caused by the temperature variance divergence under neutral conditions.

The normalized frequency corresponding to the spectral peak was derived from the minimum of Eq. (9) and given as $f_{max} = [c_{11}(p_4 p_5 - 1)]^{-1/p_4}$. For the u, v, and w spectra, the spectral peak occurs at frequencies $f_{max} = 0.031$, 0.068, and 0.20, respectively. These are less than the frequencies found in Łódź under neutral conditions by Fortuniak and Pawlak (2015) whose values were 0.052–0.065, 0.15–0.17, and 0.32–0.35, respectively. Nonetheless, Högström et al. (1982) verified frequencies close to those found in this study for u and v spectra under neutral conditions in Uppsala, SE, using turbulence measurements at 8 m a.s.l. ($f_{max} = 0.032$ and 0.046, respectively). Similarly, Anderson and Verma (1985) reported f_{max} of 0.02 and 0.05 over vegetated surface, respectively. A possible explanation for the different f_{max} values could be its dependence on the measurement height that was verified over urban surfaces for spectra of the wind components and temperature (Feigenwinter et al. 1999; Roth 2000). This dependence shifts the f_{max} to the high-frequency range with increasing $z/\overline{H}$ ratio. However, the measurements carried out in Łódź showed $z/\overline{H}$ values of approximately 2.6 and 3.4, which are less than the value 3.8 from this study. Therefore, the observed difference could be associated with other factors, such as a possible underestimation of the zero-plane displacement d, since the estimation method employed by Fortuniak and Pawlak (2015) (a simple rule-of-thumb) does not consider the heterogeneous roughness elements of an urban surface (Kanda et al. 2002; Kent et al. 2017a; Kent et al. 2017b; Silveira et al. 2022). Consequently, the effective measurement height $(z - d)$ and the normalized frequency could be overestimated.

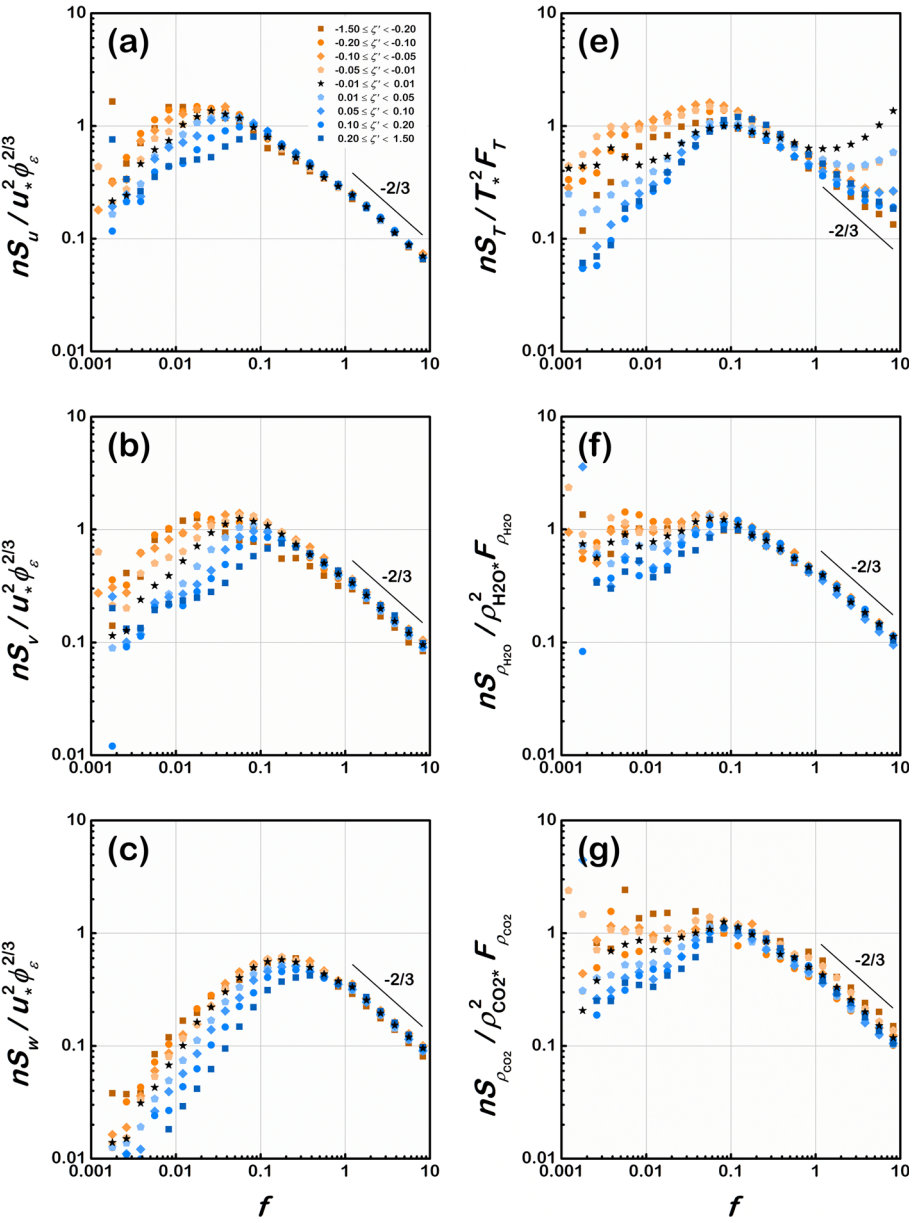

Fig. 6 Normalized spectra of (**a–c**) velocity and (**d–f**) scalar variances in São Paulo. The spectra are divided by $F_x = \phi_\varepsilon^{2/3}$ (for $x = u, v, w$) and $F_x = \phi_{N_x} \phi_\varepsilon^{-1/3}$ (for $x = T, \rho_{H2O}, \rho_{CO2}$), where ϕ_ε and ϕ_{N_x} are the similarity functions of the normalized dissipation rates of turbulent kinetic energy and half the variance of x, respectively. f is the normalized frequency and ζ' is the stability parameter. Unstable (stable) conditions are indicated by orange (blue) shading and neutral conditions are indicated by black stars. The spectral values represent the medians of the frequency bands. The short solid line indicates the − 2/3 slope in the inertial subrange ($1 < f < 10$)

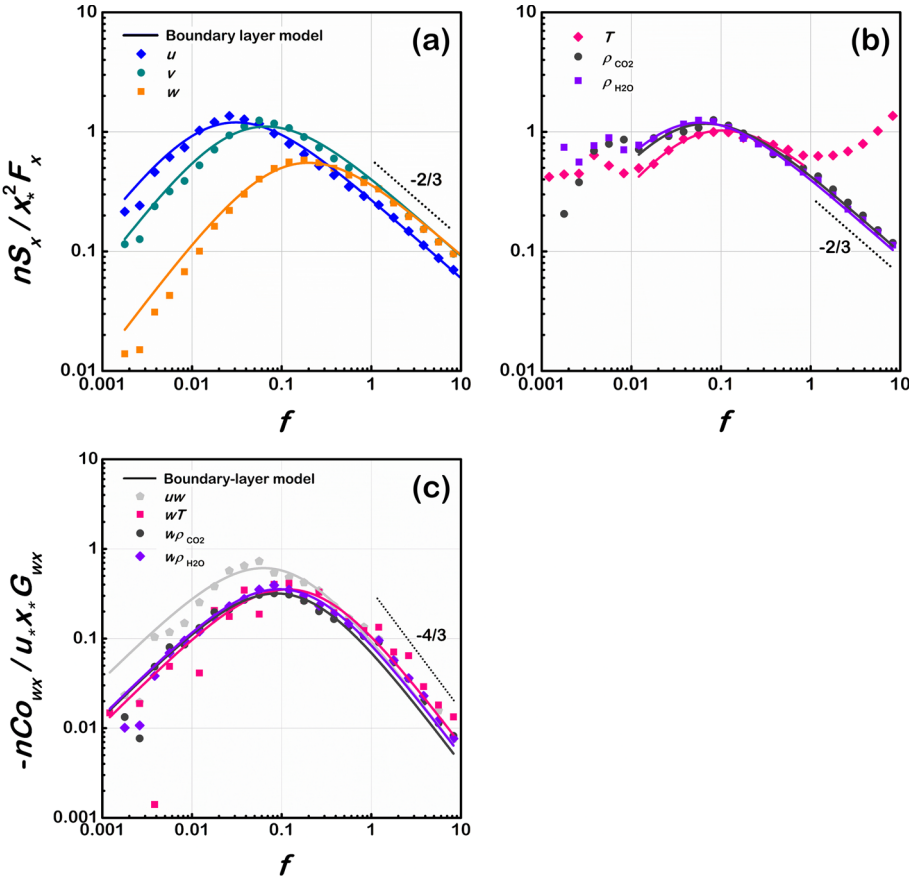

Fig. 7 Boundary-layer models for the normalized (co)spectra of (**a**) velocity, (**b**) scalars, and c fluxes under neutral conditions. f is the normalized frequency. The symbols indicate bin medians. Solid lines indicate the boundary-layer model (Eq. 9). Short dotted lines indicate the − 2/3 and − 4/3 slopes in the inertial subrange. Table 3 shows the model coefficients found in São Paulo

In particular, the model for the T spectrum was fitted in the range $0.01 < f < 1$ due to increasing in the inertial subrange. Its frequency associated to the spectral peak, $f_{\max} = 0.10$, agrees with the value of 0.12 obtained by extending for the entire range $0.001 < f < 10$ the spectral model $nS_T(n)/T_*^2 = 24.4f/(1 + 12.5f)^{5/3}$ proposed by Kaimal et al. (1972) for ideal surfaces. On the other hand, Ramamurthy and Pardyjak (2015) reported a lower frequency ($f_{\max} = 0.02$) for the T spectrum in Salt Lake City, US.

With respect to the ρ_{H2O} and ρ_{CO2} spectra, Eq. (9) can be used to predict the spectral peak location in the range $0.01 < f < 10$, whose associated frequencies ($f_{\max} = 0.059$ and 0.068, respectively) are greater than those observed by Roth et al. (2003) and Ramamurthy and Pardyjak (2015) in urban areas ($f_{\max} \approx 0.01$–0.02). Furthermore, Eq. (9) also describes the − 2/3 slope in the inertial subrange. However, the Kaimal model was inadequate for describing the scalar spectra from São Paulo in the low-frequency range, where the spectral energy densities display a minor peak between $f = 0.004$ and $f = 0.008$ (Fig. 7b). According to Ramamurthy and Pardyjak (2015), the turbulent transport of CO_2 in the ISL over (sub)urban

Table 3 Spectral and cospectral models under neutral conditions for urban areas

Boundary-layer model for $nS_x/x_*^2 F_x$

	$x=u$	$x=v$	$x=w$	$x=T$	$x=\rho_{H2O}$	$x=\rho_{CO2}$
São Paulo	$178f/(1+48f)^{5/3}$	$76f/(1+22f)^{5/3}$	$12.7f/(1+7.51f)^{5/3}$	$46f/(1+14.5f)^{5/3}$	$94f/(1+25.6f)^{5/3}$	$77f/(1+22f)^{5/3}$
	$R^2_{adj}=0.98$	$R^2_{adj}=0.98$	$R^2_{adj}=0.99$	$R^2_{adj}=0.89$	$R^2_{adj}=0.99$	$R^2_{adj}=0.98$
	$f_{max}=0.031$	$f_{max}=0.068$	$f_{max}=0.20$	$f_{max}=0.10$ $0.01<f<1$	$f_{max}=0.059$ $f>0.01$	$f_{max}=0.068$ $f>0.01$
Łódź-Lipowa[a]	$45f/\left(1+140f^{5/3}\right)$	$9.4f/\left(1+23f^{5/3}\right)$	$2.5f/\left(1+8.0f^{5/3}\right)$	–	–	–
Łódź-Narutowicza[a]	$44f/\left(1+145f^{5/3}\right)$	$9.7f/\left(1+25f^{5/3}\right)$	$2.8f/\left(1+8.2f^{5/3}\right)$	–	–	–
	$f_{max}=0.052$–0.065	$f_{max}=0.15$–0.17	$f_{max}=0.32$–0.35			
Uppsala[b]	$86.60f/(1+29.62f)^{5/3}$	$18.58f/(1+10.29f)^{5/3}$	$3.07f/(1+3.17f)^{5/3}$	–	–	–
	$f_{max}=0.053$, $z=50$ m	$f_{max}=0.24$, $z=50$ m	$f_{max}=0.54$, $z=50$ m			

Boundary-layer model for $nCo_{wx}/u_* x_* G_{wx}$

	$x=u$	$x=T$	$x=\rho_{H2O}$	$x=\rho_{CO2}$
São Paulo	$36f/(1+11.8f)^{7/3}$	$11f/(1+6.4f)^{7/3}$	$13.9f/(1+7.9f)^{7/3}$	$13f/(1+8.5f)^{7/3}$
	$R^2_{adj}=0.95$	$R^2_{adj}=0.86$	$R^2_{adj}=0.98$	$R^2_{adj}=0.95$
	$f_{max}=0.064$	$f_{max}=0.12$	$f_{max}=0.095$	$f_{max}=0.088$
Łódź-Lipowa[a]	$10.2f/(1+7.4f)^{7/3}$	–	–	–

Table 3 (continued)

Boundary-layer model for $nCo_{wx}/u_* x_* G_{wx}$				
	$x=u$	$x=T$	$x=\rho_{H2O}$	$x=\rho_{CO2}$
Łódź-Narutowicza[a]	$12.9f/(1+9.5f)^{7/3}$ $f_{max} \sim 0.08$	–	–	–

$nS_x/x_*^2 F_x$ is the normalized spectrum of x; $nCo_{wx}/u_* x_*$ is the normalized cospectrum of the x flux; f is the normalized frequency; f_{max} is the (co)spectral peak frequency; R^2_{adj} is the adjusted R-squared; z is the measurement height above the surface level. The boundary-layer models are based on Kaimal et al. (1972)

[a] Fortuniak and Pawlak (2013)

[b] Högström et al. (1982)

areas is significantly influenced by non-local effects and is characterized by multiple peaks. In addition, they suggested that these non-local effects are related to advection, the distribution of roughness elements (or sources), and urban heat island effects.

3.8 Normalized Cospectra

Normalized cospectra were divided by the similarity functions G_{wx} obtained in São Paulo to remove the stability dependence in the inertial subrange and the parameter ζ' was distributed into 9 stability ranges, analogous to the spectra. In the inertial subrange, the normalized cospectra converge and their intensities decay with an exponent on the order of $-$ 4/3 (as shown in Table 1). Under stable conditions, the cospectral peaks depend on ζ' and shift to higher frequencies with increasing stability. Under unstable conditions the cospectra is within a narrow range, where cospectral peaks apparently overlap, coinciding with the cospectrum under neutral conditions (Fig. 8). Other studies in (sub)urban areas have documented similar

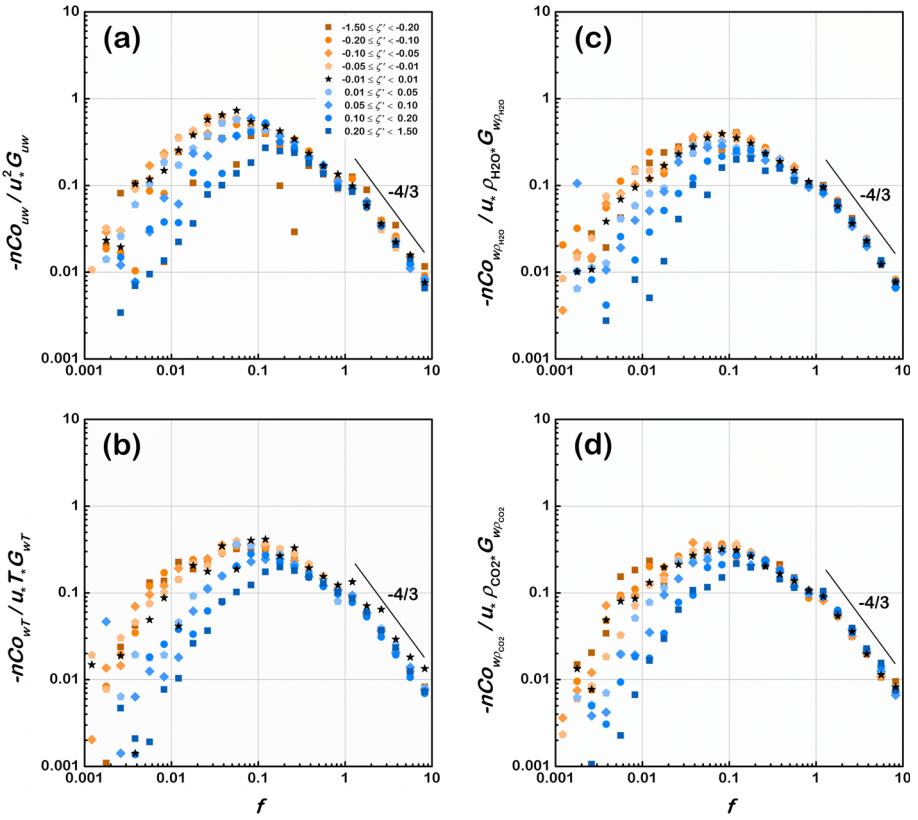

Fig. 8 Normalized cospectra of (**a**) momentum and (**b–d**) scalar fluxes in São Paulo. The cospectra are divided by the similarity functions of the normalized dissipation rates G_{wx} (where $x = u$, T, ρ_{H2O}, ρ_{CO2}). f is the normalized frequency and ζ' the stability parameter. Unstable (stable) conditions are indicated by orange (blue) shading and neutral conditions are indicated by black stars. The cospectral values represent the medians of the frequency bands. The short solid line indicates the $-$ 4/3 slope in the inertial subrange ($1 < f < 10$)

results for the cospectra of momentum, heat, humidity, and CO_2 fluxes (Roth and Oke 1993; Feigenwinter et al. 1999; Fortuniak and Pawlak 2015; Ramamurthy and Pardyjak 2015).

From the normalized cospectra under neutral conditions, Eq. (9) was fitted to the data to determine the frequency (f_{max}) associated with the energy peak. The fit results are provided in Table 3. Generally, the normalized cospectra of both momentum and scalar fluxes can be described in São Paulo by setting the exponents $p_4 = 1$ and $p_5 = 7/3$ over the entire frequency range (cf. Kaimal et al. 1972) (Fig. 7c). In addition, the normalized cospectra of water vapor and CO_2 have practically the same shape (or parameters) and peak frequencies. A similar result was observed by Ramamurthy and Pardyjak (2015) in Salt Lake City under neutral conditions. Ohtaki and Matsui (1982) and Anderson and Verma (1985) reported analogous behavior in rural areas for water vapor and CO_2 cospectrum. Regarding to the momentum flux, Fortuniak and Pawlak (2015) also found exponents $p_4 = 1$ and $p_5 = 7/3$ to describe the normalized cospectrum in Łódź, as proposed by Kaimal et al. (1972). On the other hand, Feigenwinter et al. (1999) verified a disagreement between the normalized cospectrum for momentum and the Kaimal model in Basel (at height $z/\overline{H} = 3.2$) under neutral conditions.

The peak frequencies of the scalar flux cospectra in São Paulo ($f_{max} \approx 0.09$–0.1) display values greater than those observed in Salt Lake City under neutral conditions ($f_{max} \approx 0.02$–0.03). However, they agree with the value of 0.09 found for ideal surfaces (Kaimal et al. 1972). The cospectral peak for the momentum flux occurs at $f_{max} = 0.064$. This value is slightly less than the frequency (~ 0.08) found in Łódź by Fortuniak and Pawlak (2015) (Table 3). In addition, by considering that the cospectra under unstable conditions are close to the cospectrum under neutral conditions, it is plausible to conclude that the f_{max} estimates for heat and momentum flux cospectra in São Paulo are in agreement with results found in Basel (0.16 and 0.085, respectively) (Feigenwinter et al. 1999).

4 Summary and Conclusions

The objective of this study was to observationally investigate the spectral properties of the turbulence on São Paulo Megacity. To achieve this goal, turbulence measurements of wind velocity components, temperature, and water vapor and carbon dioxide densities were carried out at 25–26 m a.s.l. between 2009 and 2017 in a suburban area of the São Paulo Megacity, the largest metropolitan region in Brazil. The normalized spectra and cospectra of the atmospheric variables were determined and analyzed within the Monin–Obukhov similarity theory framework. The main findings are summarized as follows:

1) Under neutral conditions, S_v/S_u tends to the 4/3 isotropic ratio in the inertial subrange. On the other hand, S_w/S_u deviates from the expected value in urban areas. A possible explanation for this departure may be the local imbalance of turbulent kinetic energy. However, this hypothesis needs a more thorough investigation.
2) The normalized spectra of the wind components, temperature, and density of water vapor and carbon dioxide follow the Kolmogorov law, displaying a slope on the order of − 2/3 in the inertial subrange. Similarly, the normalized cospectra of the vertical fluxes of momentum, heat, water vapor, and CO_2 decay in the inertial subrange in accordance with the − 4/3 power law.
3) The spectral and cospectral peaks depend on the stability and shift to higher frequencies as the stability parameter ζ' increases. Nonetheless, this dependence is not clear for the normalized spectra of ρ_{H2O} and ρ_{CO2} due to the influence of non-local effects in the low-frequency range. Under unstable conditions, the normalized cospectra are within a

narrow range at low frequencies close to the cospectral curve for neutral conditions and the peak dependence on ζ' is unclear.

4) The normalized cospectra of water vapor and CO_2 flux are practically identical under neutral conditions, displaying the same shape and peak frequency. On the other hand, the cospectral energy density of heat flux is about 5/3 greater than that of passive-gas cospectra in the inertial subrange in São Paulo.
5) The behavior of the normalized dissipation rates of the turbulent kinetic energy and of half the variance of the passive gas density as a function of ζ', divided by their neutral condition values, can be described in urban areas by similarity functions based on the local equilibrium hypothesis. Moreover, the results from this study indicate that $F_{\rho_{H2O}} \approx F_{\rho_{CO2}}$ in urban areas. On the other hand, the commonly used functions for the normalized dissipation rate of temperature variance do not adequately describe urban data, where functions in the form $F_T(\zeta') = c_8 + c_9|\zeta'|^{-|p_3|}$ are more appropriate.
6) The normalized dissipation rates of the momentum and scalar fluxes G_{wx} are close to unity under unstable conditions, in agreement with Kaimal et al.'s (1972) proposal. Under stable conditions, the dependence of G_{wx} on stability is described by linear functions in São Paulo. In addition, the results indicate that the relationship $\alpha_{wT} = \alpha_{w\rho_{H2O}} = \alpha_{w\rho_{CO2}}$ of the cospectral constants for scalar fluxes may be valid over urban surfaces.
7) The systematic deviations of the (co)spectral constants found in urban areas from the values established in the literature may be associated with the imbalance between local dissipation and production terms of TKE and variance.

Generally, it is important to highlight that turbulence spectra and cospectra over urban surfaces are poorly documented in the literature, especially for scalars. The few observational studies significatively limit the intercomparison of the results, as well as to draw conclusions regarding the spectral properties of the turbulence in urban environments. This limitation emphasizes the importance of the present study for obtaining a better understanding of the turbulent exchange processes of mass, heat, and momentum in the urban boundary layer.

Appendix 1: Averaging Timescale Test

Determining the optimal averaging timescale provides more accurate estimate of turbulent fluxes and is an objective way to remove contamination from (sub)mesoscale fluctuations (Stiperski et al. 2019). The multiresolution decomposition (MRD) allows to identify the 'gap region' that separates mesoscale from turbulent transport (Vickers and Mahrt 2003).

Following Vickers and Mahrt's (2003) methodology, the optimal averaging timescale (i.e., the beginning of the gap region) was determined by applying the MRD to turbulence measurements carried out at PM IAG from June 1 to 30, 2015. These one-month long time series were split in 1 h blocks. Only the blocks approved in the DQC procedures indicated in Sect. 2.2 were used in the MRD analysis. To assess the averaging timescale corresponding to unstable and stable conditions, the blocks were organized by daytime (0800–1600 LT, LT = UTC–3 h) and night-time (1800–0600 LT), respectively. To avoid nonstationarity effects, measurements during transition periods (0600–0800 LT and 1600–1800 LT) were removed. The resultant dataset used in the analysis encompassed 130 stable and 66 unstable 1 h blocks over 11 days. In addition, the central tendency of the cospectra was measured through the median, which is unaffected by extreme values and provides a plausible averaging timescale for the whole dataset. The optimal averaging timescale is achieved when the heat flux cospectrum changes

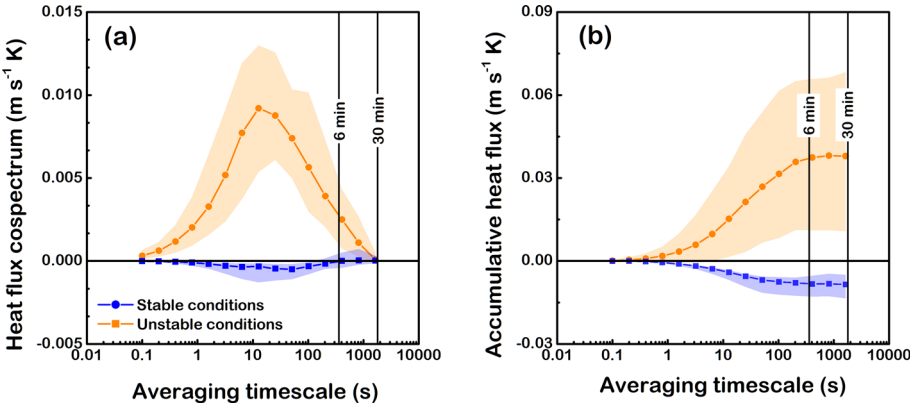

Fig. 9 Results of the MRD analysis for one-month long time series of turbulence measurements selected randomly from the entire data set. Heat flux cospectrum are indicated by (**a**) and the accumulative heat flux by (**b**). Solid squares and circles indicate the medians for stable and unstable conditions, respectively. The shading indicates the range between the 25th and 75th percentiles. The vertical solid lines indicate the optimal averaging timescales of 6 min and 30 min

sign or, equivalently, when the cumulative heat flux reaches its first peak or levels off after the first peak (Vickers and Mahrt 2003; Stiperski et al. 2019).

The results showed in Fig. 9 indicate the heat fluxes were fully sampled for a 30 min averaging timescale under unstable conditions. For stable conditions, the gap region appears to begin at 6 min and indicates that this could be a more appropriate averaging timescale for flux estimates (Fig. 9). However, the difference between 6 min and 30 min average values of heat fluxes over the one-month period ($-\ 6.01 \times 10^{-3}$ W m^{-2} and $-\ 6.08 \times 10^{-3}$ W m^{-2}, respectively) was of 1%, in agreement with the differences less than 5% verified by Vickers and Mahrt (2003) under stable conditions for the average values of heat fluxes estimated using the optimal averaging timescale and 30 min blocks.

These results indicate that the mesoscale contamination did not affect the heat fluxes properties in the PM IAG site. Therefore, it seems plausible to assume that an averaging timescale of 30 min is appropriate to estimate the spectral properties of the turbulence in the present study.

Appendix 2: Dissipation Rates of Turbulent Kinetic Energy

See Fig. 10.

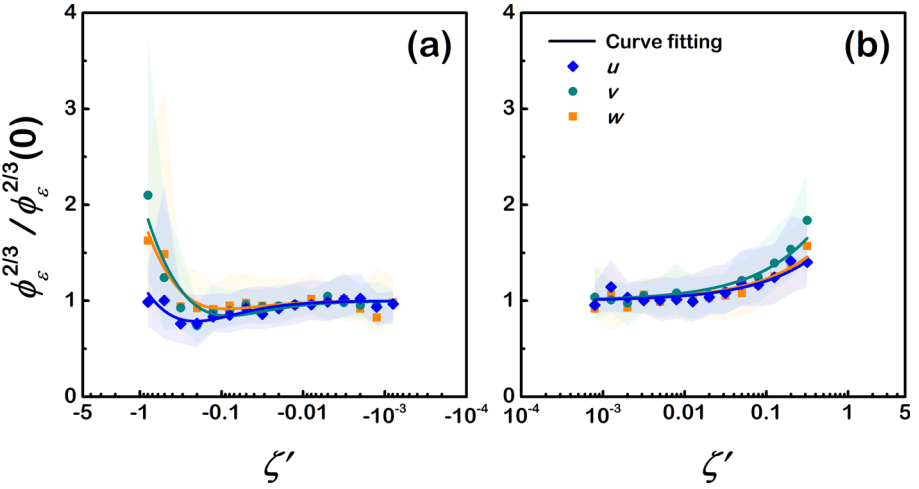

Fig. 10 Normalized dissipation rate of turbulent kinetic energy in the direction of the u, v, and w velocity components. $\phi_\varepsilon^{2/3}(0)$ is the imbalance factor. ζ' is the stability parameter. The symbols and shading indicate the median and range between the 25th and 75th percentiles of stability bins, respectively. Table 2 shows the similarity curves for São Paulo of each velocity component. The fitting procedure is described in Sect. 3.5

Acknowledgements This study is part of the MCITY BRAZIL and BIOMASP+ projects sponsored by the Brazilian Research Foundations FAPESP (2011/50178-5; 2020/07141-2), FAPERJ (E26/111.620/2011; E26/103.407/2012), CNPq (309079/2013-6; 305357/2012-3; 462734/2014-5; 304786/2018-7), CAPES (001), and the Slovenian Research Agency (LI-4154A; L2-5457C; L2-6762C).

Author Contribution L.C.S. and A.P.O. wrote and reviwed the main manuscript text. G.C. and M.P.S. contributed to data acquisition. A.P.O. and A.F. ensured that questions related to the accuracy or integrity of any part of the work were appropriately investigated and resolved.

Funding Conselho Nacional de Desenvolvimento Científico e Tecnológico,309079/2013-6,305357/2012-3,462734/2014-5304786/2018-7,309079/2013-6,305357/2012-3,462734/2014-5304786/2018-7,309079/2013-6,305357/2012-3,462734/2014-5304786/2018-7,Coordenação de Aperfeiçoamento de Pessoal de Nível Superior, Slovenian Research Agency,LI-4154A,L2-5457C,L2-6762C,LI-4154A,L2-5457C,L2-6762C,LI-4154A,L2-5457C,L2-6762C,Fundação de Amparo à Pesquisa do Estado de São Paulo,2011

Declarations

Conflict of interest The authors declare no competing interests.

References

Anderson DE, Verma SB (1985) Turbulence spectra of CO_2, water vapor, temperature and wind velocity fluctuations over a crop surface. Boundary-Layer Meteorol 33:1–14

Andersson A, Sjöblom A, Sahlée E, Falck E, Rutgersson A (2019) Enhanced air-sea exchange of heat and carbon dioxide over a high arctic fjord during unstable very-close-to-neutral conditions. Boundary-Layer Meteorol 170:471–488

Andreas EL (1987) On the kolmogorov constants for the temperature-humidity cospectrum and the refractive index spectrum. J Atmos Sci 44:2399–2406

Babić K, Rotach MW (2018) Turbulence kinetic energy budget in the stable boundary layer over a heterogeneous surface. Q J R Meteorol Soc 144:1045–1062
Barlow JF (2014) Progress in observing and modelling the urban boundary layer. Urban Clim 10:216–240
Cheng XL, Weng BL, Hu F, Zhu R (2010) Kolmogorov constants of atmospheric turbulence over a homogeneous surface. Atmos Ocean Sci Lett 3:195–200
Cheng Y, Sayde C, Li Q, Basara J, Selker J, Tanner E, Gentine P (2017) Failure of Taylor's hypothesis in the atmospheric surface layer and its correction for eddy-covariance measurements. Geophys Res Lett 44:4287–4295
Christen A, Rotach MW, Vogt R (2009) The budget of turbulent kinetic energy in the urban roughness sublayer. Boundary-Layer Meteorol 131:193–222
Clarke JF, Ching JKS, Godowitch JM (1982) An experimental study of turbulence in an urban environment. Tech Rep US EPA, Research Triangle Park, NC, NMS PB 226085, 155 pp
Dyer AJ, Bradley EF (1982) An alternative analysis of flux-gradient relationships at the 1976 ITCE. Boundary-Layer Meteorol 22:3–19
Dyer AJ, Hicks BB (1982) Kolmogoroff constants at the 1976 ITCE. Boundary-Layer Meteorol 22:137–150
Falabino S, Trini Castelli S (2017) Estimating wind velocity standard deviation values in the inertial sublayer from observations in the roughness sublayer. Meteorol Atmos Phys 129:83–98
Feigenwinter C, Vogt R, Parlow E (1999) Vertical structure of selected turbulence characteristics above an urban canopy. Theor Appl Climatol 62:51–63
Foken T (2006) 50 Years of the monin-obukhov similarity theory. Boundary-Layer Meteorol 119:431–447
Foken T, Leuning R, Oncley SR, Mauder M, Aubinet M (2012) Corrections and data quality control. In: Aubinet M, Vesala T, Papale D (eds) Eddy covariance: a practical guide to measurement and data analysis. Springer, Dordrecht, pp 85–131
Fortuniak K, Pawlak W (2015) Selected spectral characteristics of turbulence over an urbanized area in the centre of Łódź, Poland. Boundary-Layer Meteorol 154:137–156
Frenzel P, Vogel C (2001) Further studies of atmospheric turbulence in layers near the surface: scaling the TKE budget above the roughness sublayer. Boundary-Layer Meteorol 99:173–206
Frisch U (1995) Turbulence: The Legacy of A.N. Kolmogorov. Cambridge University Press, Cambridge, UK
Garbero V, Salizzoni P, Soulhac L (2010) Experimental study of pollutant dispersion within a network of streets. Boundary-Layer Meteorol 136:457–487
Hackerott JA, Bakhoday Paskyabi M, Reuder J, Oliveira AP, Kral ST, Marques Filho EP, Mesquita MS, Camargo R (2017) A surface-layer study of the transport and dissipation of turbulent kinetic energy and the variances of temperature, humidity and co_2. Boundary-Layer Meteorol 165:211–231
Högström U, Bergström H, Alexandersson H (1982) Turbulence characteristics in a near neutrally stratified urban atmosphere. Boundary-Layer Meteorol 23:449–472
Högström U (1988) Non-dimensional wind and temperature profiles in the atmospheric surface layer: a re-evaluation. Boundary-Layer Meteorol 42:55–78
Högström U (1990) Analysis of turbulence structure in the surface layer with a modified similarity formulation for near neutral conditions. J Atmos Sci 47:1949–1972
Högström U (1996) Review of some basic characteristics of the atmospheric surface layer. Boundary-Layer Meteorol 78:215–246
IBGE (2018) Brazilian Institute of Geography and Statistics. Retrieved from: https://agenciadenoticias.ibge.gov.br/en/agencia-press-room/2185-news-agency/releases-en/22385-ibge-releases-population-estimates-of-municipalities-for-2018. Accessed July 2023
Iwata T, Yoshikawa K, Higuchi Y, Yamashita T, Kato S, Ohtaki E (2005) The spectral density technique for the determination of Co_2 flux over the ocean. Boundary-Layer Meteorol 117:511–523
Kaimal JC, Wyngaard JC, Izumi Y, Coté OR (1972) Spectral characteristics of surface-layer turbulence. Q J R Meteorol Soc 98:563–589
Kaimal JC, Gaynor JE (1983) The boulder atmospheric observatory. J Clim Appl Meteorol 22:863–880
Kaimal JC, Kristensen L (1991) Time series tapering for short data samples. Boundary-Layer Meteorol 57:187–194
Kanda M, Moriwaki R, Roth M, Oke T (2002) Area-averaged sensible heat flux and a new method to determine zero-plane displacement length over an urban surface using scintillometry. Boundary-Layer Meteorol 105:177–193
Kent CW,Grimmond S, Barlow J,Gatey D, Kotthaus S,Lindberg F, Halios CH(2017a) Evaluation ofUrban Local-ScaleAerodynamic Parameters:Implications for theVertical Profile of WindSpeed and for SourceAreas. Boundary-LayerMeteorol 164:183–213
Kent CW, Grimmond S,1ovrvenGatey D (2017b)Aerodynamic roughnessparameters in cities:Inclusion of vegetation. JWind Eng Ind Aerodyn169:168–176

Kolmogorov AN (1991) The local structure of turbulence in incompressible viscous fluid for very large Reynolds numbers. Proc R Soc Lond A 434:9–13
Larsén XG, Larsen SE, Petersen EL, Mikkelsen TK (2021) A model for the spectrum of the lateral velocity component from mesoscale to microscale and its application to wind-direction variation. Boundary-Layer Meteorol 178:415–434
Li X, Zimmerman N, Princevac M (2008) Local imbalance of turbulent kinetic energy in the surface layer. Boundary-Layer Meteorol 129:115–136
Liu L, Shi Y, Zhang Z, Hu F (2023) Variability of turbulence dispersion characteristics during heavy haze process: a case study in Beijing. J Environ Sci 124:440–450
Lundquist JK, Shinn JH, Gouveia F (2004) Observations of turbulent kinetic energy dissipation rate in the urban environment. In: Symposium on Planning, Nowcasting, and Forecasting in the Urban Zone, Seattle, WA, January 10–15, 5 pp
Mahrt L (1998) Flux sampling errors for aircraft and towers. J Atmos Ocean Technol 15:416–429
Moreira GA, Oliveira AP, Codato G, Sánchez MP, Tito JV, Silva LAH, Silveira LC, Silva JJ, Lopes FJS, Landulfo E (2022) Assessing spatial variation of PBL height and aerosol layer aloft in São Paulo megacity using simultaneously two lidar during winter 2019. Atmos 13:611
Mortarini L, Anfossi D (2015) Proposal of an empirical velocity spectrum formula in low-wind speed conditions. Q J R Meteorol Soc 141:85–97
Mortarini L, Maldaner S, Moor LP, Stefanello MB, Acevedo O, Degrazia G, Anfossi D (2016) Temperature auto-correlation and spectra functions in low-wind meandering conditions. Q J R Meteorol Soc 142:1881–1889
Norman M, Rutgersson A, Sørensen LL, Sahlée E (2012) Methods for estimating air-sea fluxes of CO_2 using high-frequency measurements. Boundary-Layer Meteorol 144:379–400
Nilsson E, Lohou F, Lothon M, Pardyjak E, Mahrt L, Darbieu C (2016) Turbulence kinetic energy budget during the afternoon transition—Part 1: observed surface TKE budget and boundary layer description for 10 intensive observation period days. Atmos Chem Phys 16:8849–8872
Ohtaki E (1982) The Kolmogorov constant for carbon dioxide in the atmospheric surface layer over a paddy field. Boundary-Layer Meteorol 23:153–159
Ohtaki E (1985) On the similarity in atmospheric fluctuations of carbon dioxide, water vapor and temperature over vegetated fields. Boundary-Layer Meteorol 32:25–37
Ohtaki E, Matsui T (1982) Infrared device for simultaneous measurement of fluctuations of atmospheric carbon dioxide and water vapor. Boundary-Layer Meteorol 24:109–119
Oikawa S, Meng Y (1995) Turbulence characteristics and organized motion in a suburban roughness sublayer. Boundary-Layer Meteorol 74:289–312
Oliveira AP, Bornstein RD, Soares J (2003) Annual and diurnal wind patterns in the city of São Paulo. Water Air Soil Pollut 3:3–15
Oliveira AP, Marques Filho EP, Ferreira MJ et al (2020) Assessing urban effects on the climate of metropolitan regions of Brazil—preliminary results of the MCITY project. Exploratory Environ Sci Res 1:38–77
Oncley SP, Friehe CA, Larue JC, Businger JA, Itsweire EC, Chang SS (1996) Surface-layer fluxes, profiles, and turbulence measurements over uniform terrain under near-neutral conditions. J Atmos Sci 53:1029–1044
Pahlow M, Parlange MB, Porté-Agel F (2001) On monin-obukhov similarity in the stable atmospheric boundary layer. Boundary-Layer Meteorol 99:225–248
Ramamurthy P, Pardyjak, ER (2015) Turbulent Transport of Carbon Dioxide over a Highly Vegetated Suburban Neighbourhood. Boundary-Layer Meteorol 157:461-479
Rebmann C, Kolle O, Heinesch B, Queck R, Ibrom A, Aubinet M (2012) Data acquisition and flux calculations. In: Aubinet M, Vesala T, Papale D (eds) Eddy covariance: a practical guide to measurement and data analysis. Springer, Dordrecht, pp 59–83
Ribeiro FND, Oliveira AP, Soares J, Miranda RM, Barlage M, Chen F (2018) Effect of sea breeze propagation on the urban boundary layer of the metropolitan region of Sao Paulo, Brazil. Atmos Res 214:174–188
Rotach MW (1994) Determination of the zero-plane displacement in an urban environment. Boundary-Layer Meteorol 67:187–193
Rotach MW (1995) Profiles of turbulence statistics in and above urban street canyon. Atmos Environ 29:1473–1486
Roth M, Oke TR (1993) Turbulent transfer relationships over an urban surface. i spectral characteristics. Q J R Meteorol Soc 119:1071–1104
Roth M (2000) Review of atmospheric turbulence over cities. Q J R Meteorol Soc 126:941–990
Roth M, Salmond J, Satyanarayana A, Christen A, Vogt R, Oke TR (2003) Turbulence characteristics, similarity and CO_2 (co)spectra over an urban canopy. In: Fifth international conference on urban climate, 3 pp

Roth M, Salmond JA, Satyanarayana ANV (2006) Methodological considerations regarding the measurement of turbulent fluxes in the urban roughness sublayer: the role of scintillometery. Boundary-Layer Meteorol 121:351–375

Roy S, Sentchev A, Schmitt FG, Augustin P, Fourmentin M (2021) Impact of the nocturnal low-level jet and orographic waves on turbulent motions and energy fluxes in the lower atmospheric boundary layer. Boundary-Layer Meteorol 180:527–542

Sánchez MP, Oliveira AP, Varona RP, Tito JV, Codato G, Ynoue RY, Ribeiro FND, Marques Filho EP, Silveira LC (2022) Observational investigation of the low-level jets in the metropolitan region of São Paulo. Brazil Earth Space Sci. https://doi.org/10.1029/2021EA002190

Sánchez MP, Oliveira AP, Varona RP, Vito JV, Codato G, Ribeiro FND, Marques Filho EP, Silveira LC (2020) Rawinsonde-based analysis of the urban boundary layer in the metropolitan region of São Paulo. Brazil Earth Space Sci. https://doi.org/10.1029/2019EA000781

Silveira LC, Oliveira AP, Sánchez MP, Codato G, Ferreira MJ, Marques Filho EP, Božnar MZ, Mlakar P (2022) Observational Investigation of the Statistical Properties of Surface-Layer Turbulence in a Suburban Area of São Paulo, Brazil: Objective Analysis of Scaling-Parameter Accuracy and Uncertainties. Boundary-Layer Meteorol 185:161–195

Sjöblom A, Smedman A (2002) The turbulent kinetic energy budget in the marine atmospheric surface layer. J Geophys Res. https://doi.org/10.1029/2001JC001016

Sjöblom A, Smedman AS (2004) Comparison between eddy-correlation and inertial dissipation methods in the marine atmospheric surface layer. Boundary-Layer Meteorol 110:141–164

Smedman-Högström AS (1973) Temperature and humidity spectra in the atmospheric surface layer. Boundary-Layer Meteorol 3:329–347

Stiperski I, Calaf M, Rotach M (2019) Scaling, anisotropy, and complexity in near-surface atmospheric turbulence. J Geophys Res Atmos 124:1428–1448

Stuck M, Vidal A, Torres P, Nagib HM, Wark C, Vinuesa R (2021) Spectral-element simulation of the turbulent flow in an urban environment. Appl Sci 11:6472

Stull RB (1988) An Introduction to Boundary Layer Meteorology. Kluwer Academic Publishers, Dordrecht, NL

Su HB, Schmid HP, Grimmond CSB, Vogel CS, Oliphant AJ (2004) Spectral characteristics and correction of long-term eddy-covariance measurements over two mixed hardwood forests in non-flat terrain. Boundary-Layer Meteorol 110:213–253

Taleghani M, Sailor D, Ban-Weiss GA (2016) Micrometeorological simulations to predict the impacts of heat mitigation strategies on pedestrian thermal comfort in a Los Angeles neighborhood. Environ Res Lett 11:024003

Tampieri F, Maurizi A, Viola A (2009) An Investigation on Temperature Variance Scaling in the Atmospheric Surface Layer. Boundary-Layer Meteorol 132:31–42

Toda M, Sugita M (2003) Single level turbulence measurements to determine roughness parameters of complex terrain. J Geophys Res 108:4363

Toparlar Y, Blocken B, Vos P, van Heijst GJF, Janssen WD, van Hooff T, Montazeri H, Timmermans HJP (2015) CFD simulation and validation of urban microclimate: a case study for Bergpolder Zuid, Rotterdam. Build Environ 83:79–90

Umezaki AS, Ribeiro FND, Oliveira AP, Soares J, Miranda RM (2020) Numerical Characterization of Spatial and Temporal Evolution of Summer Urban Heat Island Intensity in São Paulo. Brazil Urban Clim 32:100615

Verma SB, Anderson DE (1984) Kolmogorov constants for CO_2, wind velocity, air temperature, and humidity fluctuations over a crop surface. Boundary-Layer Meteorol 28:161–167

Vickers D, Mahrt L (1997) Quality control and flux sampling problems for tower and aircraft data. J Atmos Oceanic Technol 14:512–526

Vickers D, Mahrt L (2003) The Cospectral Gap and Turbulent Flux Calculations. J Atmos Oceanic Technol 20:660–672

Westcott N (1989) Influence of mesoscale winds on the turbulent structure of the urban boundary layer over St. Louis Boundary-Layer Meteorol 48:283–292

Wilczak JM, Oncley SP, Stage SA (2001) Sonic anemometer tilt correction algorithms. Boundary-Layer Meteorol 99:127–150

Wyngaard JC, Coté OR (1971) The budgets of turbulent kinetic energy and temperature variance in the atmospheric surface layer. J Atmos Sci 28:190–201

Wyngaard JC, Coté OR (1972) Cospectral similarity in the atmospheric surface layer. Q J R Meteorol Soc 98:590–603

Wyngaard JC (2010) Turbulence in the Atmosphere. Cambridge University Press, New York, US

Zhang H, Chen J, Park SU (2001) Turbulence structure in unstable conditions over various surfaces. Boundary-Layer Meteorol 100:243–261

Publisher's Note Springer Nature remains neutral with regard to jurisdictional claims in published maps and institutional affiliations.

Springer Nature or its licensor (e.g. a society or other partner) holds exclusive rights to this article under a publishing agreement with the author(s) or other rightsholder(s); author self-archiving of the accepted manuscript version of this article is solely governed by the terms of such publishing agreement and applicable law.